Vacuolar Phosphatidylinositol 3,4,5-trisphosphate controls fusion through binding Vam7, and membrane microdomain assembly

Chi Zhang [1,3], Jorge D. Calderin [1,3], Aliasgar Topiwalla [1], Ved Shah [1], Jahnavi M. Karat [1], Charlie T. Knapp [1], Razeen Ahmed [1], Daniel Grudzien [1], Elizabeth Williamson [2], and Rutilio A. Fratti [1,2]

1. Department of Biochemistry, University of Illinois Urbana-Champaign, Urbana, IL 61801, USA
2. Center for Biophysics & Quantitative Biology., University of Illinois Urbana-Champaign, Urbana, IL 61801, USA
3. These authors contributed equally

Correspondence to Rutilio A. Fratti: rfratti@illinois.edu

Running title: Vacuole Fusion Regulation by PI(3,4,5)P_3.

Keywords: Grp1-PH, Ypt7, SNARE, PIP3, HOPS, Vps33, PTEN, Vps34

Abstract

Membrane trafficking is regulated by phosphoinositides (PI) and their modification. The endolysosomal pathway is controlled by PI3P, PI(4,5)P_2 and PI(3,5)P_2, whereas a role for PI(3,4,5)P_3 is less clear. We report that yeast vacuoles produce PI(3,4,5)P_3 through Vps34 activity. In vitro assays showed that dioctanoyl (C8) PI(3,4,5)P_3 or the PI(3,4,5)P_3-binding domain Grp1-PH blocked fusion. Furthermore, modifying endogenous PI(3,4,5)P_3 with the phosphatase PTEN abolished fusion. Fluorescence microscopy showed that PI(3,4,5)P_3 was present at the plasma membrane and the vertex microdomains of vacuoles. PI(3,4,5)P_3 staining was blocked by PTEN, C8-PI(3,4,5)P_3, the Vps34 inhibitor SAR405 and a *VPS34* temperature sensitive mutation. Importantly, blocking or eliminating PI(3,4,5)P_3 prevented the vertex enrichment of Ypt7 and the HOPS subunit Vps33. Finally, we show that the SNARE Vam7 binds PI(3,4,5)P_3 and that both Grp1-PH and PTEN displaced it from membranes to block trans-SNARE pairing. Our results demonstrate that vacuolar PI(3,4,5)P_3 coordinates vertex assembly and SNARE function.

Introduction

Membrane trafficking and fusion are driven by a group of conserved regulatory proteins (e.g., SNAREs) and lipids with organelle specificity. Regulatory lipids are relatively low in abundance yet carry out critical aspects of membrane trafficking (Krauss and Haucke, 2007; Lemmon, 2008; Corvera et al., 1999; Balla, 2013). These lipids include phosphoinositides (PI), phosphatidic acid (PA), diacylglycerol (DAG), sterols, and sphingolipids (Balla, 2013; Lingwood and Simons, 2010; Tu-Sekine et al., 2015; Xie et al., 2015; Starr and Fratti, 2019). PIs are glycerophospholipids with an inositol head group that can be phosphorylated at the D-3, D-4 and D-5 positions to generate seven distinct lipids whose primary function is the binding of proteins with domains that recognize specific variants. Broadly speaking, different organelles are marked by a dominant PI. Endosomes are marked by PI3P, and PI(3,5)P_2, whereas the Golgi contains PI4P, and the plasma membrane is populated by PI(4,5)P_2 and PI(3,4,5)P_3. While concentrated at characteristic organelles, biologically significant amounts can traffic to different membranes where they continue to signal and control membrane function.

The yeast vacuole/lysosome collects regulatory lipids from several pathways and continues to modify PIs to control homotypic vacuole fusion, vacuole fission and autophagic flux (Starr and Fratti, 2019; Bonangelino et al., 2002; Posor et al., 2022). Homotypic vacuole fusion can be

divided into six stages each of which is driven by a spatiotemporal-specific mixture of regulatory lipids. In a stage we now call *pre-priming*, Sec18 is sequestered from inactive cis-SNARE complexes by PA (Sasser et al., 2012; Starr et al., 2016, 2019). Sec18 can transfer to cis-SNARE complexes upon the conversion of PA to DAG by the phosphatase Pah1. Once Sec18 can engage SNAREs via its adaptor protein Sec17, *priming* occurs through ATP hydrolysis, which is dependent on ergosterol and PI(4,5)P_2 through an undefined mechanism (Kato and Wickner, 2001; Mayer et al., 2000). Vacuole *tethering* occurs through the interaction of the Rab Ypt7 and its effector tethering complex HOPS (homotypic fusion and protein sorting) between partner membranes (Price et al., 2000b; a; Seals et al., 2000; Zhang et al., 2024). Ypt7 recruitment and activation is carried out by the guanine exchange factor (GEF) Mon1-Ccz1 bound to PI3P (Lawrence et al., 2014; Cabrera et al., 2014), while HOPS itself can simultaneously bind several PIs (Stroupe et al., 2006). PI3P is also essential for binding the PX domain of the soluble Qc-SNARE Vam7 and the formation of SNARE complexes during the *docking* stage (Boeddinghaus et al., 2002; Fratti and Wickner, 2007). Between docking and full content mixing, vacuoles can undergo hemifusion where only the outer leaflets of vesicles mix while leaving luminal contents are separated by the inner leaflets (Reese and Mayer, 2005; Reese et al., 2005). We and others have found that this transition requires DAG (Jun et al., 2004) and is sensitive exogenously added PI(3,5)P_2 and lysophosphatidylcholine (Miner et al., 2019; Reese and Mayer, 2005).

Roles for the remaining PIs (PI5P, PI(3,4)P_2 and PI(3,4,5)P_3) remain to be assigned in vacuole homeostasis. PI(3,4,5)P_3 is one of the most studied PIs that is mostly present at the plasma membrane where it directs many signal transduction pathways (Riehle et al., 2013). PI(3,4,5)P_3 is made by class-I PI-3-kinases p110 using PI(4,5)P_2 as a substrate (Whitman et al., 1988; Traynor-Kaplan et al., 1988; Whitman et al., 1985). PI(3,4,5)P_3 is transient and its signaling is turned off by the 3'-phosphatase PTEN or the 5'-phosphatase SHIP2 (Maehama and Dixon, 1998; Pesesse et al., 1998). While most PI(3,4,5)P_3 signaling is associated with the plasma membrane a significant amount is found on internal vesicles including the nuclear envelope and early endosome for localized Akt activation (Jethwa et al., 2015). PI(3,4,5)P_3 is also found on recycling endosomes for AP-1B dependent sorting (Fields et al., 2010), lysosomes to activate mTORC1 (Hsu et al., 2000), and trans-Golgi vesicles where PI(3,4,5)P_3 on VLDL binds to the cargo receptor Sortilin/Vps10 (Sparks et al., 2016, 2020). At the plasma membrane itself PI(3,4,5)P_3 recruits the protein kinases Akt and PDK1 to the membrane through engaging their PH domains (Dieterle et al., 2014; Levina et al., 2022).

By homology, *Saccharomyces cerevisiae* lacks p110, thus PI(3,4,5)P_3 is thought not to exist. However, the fission yeast *Schizosaccharomyces pombe* also lacks a p110 homolog, yet its class-III Vps34 homolog can make PI(3,4,5)P_3 from PI(4,5)P_2 in addition to its canonical product PI3P (Mitra et al., 2004). This suggests that a synthesis pathway for PI(3,4,5)P_3 could have evolved prior to the rise of class-I PI-3-kinases as suggested by the authors. Using *S. cerevisiae* vacuoles we examined a role for PI(3,4,5)P_3 during vacuole fusion. This study shows that PI(3,4,5)P_3 is made on vacuoles through a Vps34-dependent pathway and is required for vacuole fusion. Removing PI(3,4,5)P_3 with PTEN or blocking it with the Grp1-PH domain inhibited Ypt7-mediated vertex domain assembly leading to reduced trans-SNARE pairing and fusion. Finally, we found that Vam7 binds PI(3,4,5)P_3 and is released from membranes when the lipid is modified by PTEN or blocked by Grp1-PH.

Results

Short chain PI(3,4,5)P_3 inhibits in vitro vacuole fusion

In previous studies we have used dioctanoyl (C8) lipids to compete with endogenous sources of their long chain counterparts for binding vacuolar proteins. This revealed that C8-PA competes for Sec18 binding during pre-priming (Starr et al., 2016, 2019; Sparks et al., 2019), and that C8-PI(3,5)P_2 competes for binding to the V-ATPase subunit Vph1 and regulatory factors of Ca^{2+} transport in a phase between SNARE pairing and hemifusion (Miner et al., 2019, 2020; Zhang et al., 2022). In this study we asked whether adding C8-PI(3,4,5)$_3$ affected vacuole fusion. While this lipid has not been detected in *Saccharomyces cerevisiae*, numerous screening papers have shown that baker's yeast proteins can bind PI(3,4,5)P_3, including Vam7 (Yu and Lemmon, 2001; Gallego et al., 2010; Zhu et al., 2001; Dunn et al., 2004). This could be due to lack of specificity in these assays, or it could indicate that the lipid may exist in small transient pools that have escaped detection.

Here we added exogenous C8-PI(3,4,5)P_3 to in vitro vacuole fusion reactions and found that it potently inhibited fusion with an IC_{50} ≈80 μM **(Fig. 1A).** This showed that vacuole fusion was more sensitive to C8-PI(3,4,5)$_3$ compared to C8-PI(3,5)P_2 with an IC_{50} ≈140 μM or C8-PI3P, which failed to fully inhibit fusion at 500 μM (Miner et al., 2019). To confirm that the measured impacts were PI-specific and not an artifact of the C8 chains, we tested the C8 variants of PC, PE and PS and found that none of the bulk lipids had a significant effect on fusion **(Fig. 1B)**, indicating that the C8 chains themselves had no effect and that the PI headgroups were responsible for altering

vacuole fusion. While many PI binding domains such as the Plc1δ PH insert a loop into the membrane to stabilize their interaction (Herzog et al., 2016; Lemmon, 2008), they can also simply bind headgroups in solution, albeit with different affinities (Kavran et al., 1998; Ferguson et al., 2000). Based on this we asked if the headgroups alone could interfere with vacuole fusion. We tested the PI(3,4,5)P_3 head group Ins(1,3,4,5)P_4 as well as Ins(1,3,4)P_3 and Ins(1,3,5)P_3) and saw that they had no effect even when at 500 μM **(Fig. 1C).** This suggested that the head group alone was insufficient for vacuole fusion interference.

In order to determine which stage of fusion was affected by C8-PI(3,4,5)P_3 we performed temporal gain of resistance experiments (Mayer et al., 1996; Haas et al., 1995; Ungermann et al., 1998; Price et al., 2000b; Sasser et al., 2012; Miner et al., 2019). Inhibitors were added at different timepoints for a total of 120 min. As reactions passed a stage of fusion, e.g. Sec18-mediated priming they became resistant to inhibitors of that stage such as antibodies against Sec18 and Sec17, NEM, propranolol, or the small molecule IPA (inhibitor of priming activity) (Mayer et al., 1996; Sasser et al., 2012; Starr et al., 2016; Sparks et al., 2019). In this study we used NEM to mark the priming threshold, and GDI to mark the tethering/docking phase (Mayer and Wickner, 1997). Tethering and docking cannot be separated by this assay. Control reactions were treated with buffer alone at 27°C for the duration of the experiment, while a group of buffer-treated tubes were removed and placed on ice to mark the maximum amount of fusion for any recorded time point. We added 150 μM C8-PI(3,4,5)P_3 to individual reactions at the indicated times to see which stage would be impacted. We found that the gain of resistance curve for C8-PI(3,4,5)P_3 was shifted to the right of GDI indicating that it continued to affect fusion after Ypt7 mediated tethering **(Fig. 1D)**. This was further illustrated when the half-times of resistance were calculated. **Figure 1E** shows that the half-times of priming and docking were 5 and 12 min, respectively, whereas the half-times of C8-PI(3,4,5)P_3 was ≈26 min. This half-time is later than the $T_{1/2}$ ≈15 min we saw with PI(3,5)P_2 (Miner et al., 2019). Importantly, it should be noted that gain of resistance assay only indicates the last step the variable molecule had an effect, implying earlier stages could have been impacted as well.

PI(3,4,5)P_3-specific inhibitors block vacuole fusion

The data presented above suggested that a key PI(3,4,5)P_3-protein interaction needed for fusion could have been disrupted by exogenous C8-PI(3,4,5)P_3. To further test for a required PI(3,4,5)P_3-protein interaction we used purified GST-Grp1-PH, a PI(3,4,5)P_3-specific binding PH domain from the ARF GEF Grp1 (Guillou et al., 2007; Chen et al., 2012; Corbin et al., 2004;

Dowler et al., 2000). Sequestering PI(3,4,5)P_3 from natural binding partners with GST-Grp1-PH inhibited fusion with an average IC_{50} ≈1 μM with batch-to-batch variation. This further indicated that the lipid was present on vacuolar membranes **(Fig. 2A)**. We also tested the Grp1-PH^{K273A} mutant that has reduced PI(3,4,5)P_3 affinity (Lindsay et al., 2006; Naughton et al., 2016; Guillou et al., 2007; Yamamoto et al., 2020). We found that it only interfered with fusion with an IC_{50} ≈3.6 μM. To verify how Grp1-PH and Grp1-PH^{K237A} bound to PI(3,4,5)P_3 we performed BLI experiments. For this we used biotinylated PI(3,4,5)P_3 and PI3P bound to streptavidin biosensors which were incubated with 0, 100, 200, 400 and 800 nM Grp1-PH or Grp1-PH^{K237A}. We show that Grp1-PH bound to b-PI(3,4,5)P_3 and not to b-PI3P, whereas Grp1-PH^{K237A} failed to bind either lipid **(Fig. 2B)**. This suggests that fusion inhibition by Grp1-PH was due to binding PI(3,4,5)P_3 while the effects of Grp1-PH^{K237A} were non-specific.

To further interrogate the function of PI(3,4,5)P_3 on vacuoles we used the lipid phosphatase PTEN, which converts PI(3,4,5)P_3 to PI(4,5)P_2 (Maehama and Dixon, 1998; Lee et al., 1999). We added a dose-response curve of GST-PTEN to fusion reactions and found that it inhibited with an IC_{50} ≈60 nM **(Fig. 2C)**. This further indicated that endogenous vacuolar PI(3,4,5)P_3 affected vacuole fusion. While PTEN does have some activity against PI(3,4)P_2 and PI3P, it is 3-5 times weaker to its activity against PI(3,4,5)P_3 (Lee et al., 1999).

We then tested if PTEN and Grp1 had gain of resistance curves that matched the C8-PI(3,4,5)P_3 curve. Using the assay described above we found that the resistance curves of PTEN and Grp1-PH were shifted to the right of the GDI curve with half-times ≈25 min, which was consistent with the C8-PI(3,4,5)P_3 data **(Fig. 2D-E)**.

Next, we asked if we could protect native PI(3,4,5)P_3 from PTEN and Grp1-PH with a competitive inhibitor. We used PIT-1, a small molecule that binds to the PI(3,4,5)P_3 binding pockets of PH domains including those of AKT, PDK1, Grp1 and ARNO (Miao et al., 2010). Notably PIT-1 does not interfere with PI(3,4)P_2 interactions with TAPP1 or TAPP2, or PI(4,5)P_2 interactions with PLC. First, we tested PIT-1 alone and found that it partially inhibited fusion with an estimated IC_{50} ≈65 μM, which was near the IC_{50} for its inhibition of Akt-PH-PI(3,4,5)P_3 interactions (Miao et al., 2010) **(Fig. 2F)**. We also used the PIT-1 derivative 3,5-dimethyl PIT (DMPIT) and observed little interference with fusion **(Fig. 2F)**. The weak effects on fusion could be due to weaker affinities versus native protein-lipid affinities. Next, we tested if PIT-1 could rescue the inhibition of fusion by Grp1-PH and PTEN. Fusion reactions were first treated with 200 μM PIT-1 for 5 min at 27°C.

Reactions were stopped by placing them on ice followed by the addition of 2 μM Grp1-PH or 200 nM PTEN. Reactions were further incubated at 27°C for a total of 90 min. This showed that PIT-1 could partially reverse the effects of both Grp1-PH **(Fig. 2G)** and PTEN **(Fig. 2H)**. Similarly, DMPIT reversed Grp1-PH inhibition **(Fig. 2I)**. Interestingly, DMPIT did not reverse the effect of Grp1-PH^{K237A} further indicating that its effects on fusion, albeit miner were, a result of non-specific interactions. Finally, we found that DMPIT partially rescued the effect of PTEN **(Fig. 2J)**.

PI(3,4,5)P_3 is on the plasma membrane and on vacuoles

The inhibition of fusion by PTEN and Grp1-PH indicated that PI(3,4,5)P_3 was present on vacuoles. To visualize where PI(3,4,5)P_3 was localized on docked vacuoles we used subinhibitory concentrations of GST-Grp1-PH (150 nM) and fluorescent (CF488) anti-GST antibody. This prevented any interference caused by conjugating primary amines or free Cys with reactive dyes. Grp1 has key Lysines in the lipid binding pocket and a Cysteine next to a lipid-interacting Lys (Cronin et al., 2004; Lai et al., 2013). We found that CF488-Grp1-PH localized to vertices of docked vacuoles where essential lipids and proteins accumulate to trigger fusion **(Fig. 3A-B)** (Wang et al., 2002; Eitzen et al., 2002; Wang et al., 2003; Fratti et al., 2004; Karunakaran et al., 2012; Jun et al., 2006; Miner et al., 2019, 2020; Zhang et al., 2024). Vacuole labeling was significantly reduced with the Class-III PI-3-kinase-specific inhibitor SAR405 (Ronan et al., 2014), which signified that PI(3,4,5)P_3 production could be Vps34-dependent and not due to an unidentified Class-I homolog. This is also in accord with Vps34 production of PI(3,4,5)P_3 in fission yeast (Mitra et al., 2004).

While SAR405 reduced PI(3,4,5)P_3 signal on isolated vacuoles, a significant number of vertices stained with Grp1-PH indicating that pre-existing lipid was present on membranes. This could come from production prior to isolation as well as trafficking from the plasma membrane (Sahan et al., 2025). To test if the plasma membrane contained PI(3,4,5)P_3 we used whole cells that were treated with lyticase to digest the cell wall and permeabilize the plasma membrane, and fixed formaldehyde (Martínez-Muñoz and Peña, 2005; Pringle et al., 1991). Cells were then incubated with GST-Grp1-PH and CF488 anti-GST antibody then mounted with media containing DAPI to label nuclei. Figure 3 shows fluorescence for individual channels as well as a merged image and a heat map to show relative intensities **(Fig 3C)**. Grp1 staining intensities were quantified by ratiometric fluorescence measurements of CF488 and DAPI. This showed that untreated cells had a mean fluorescence that was significantly greater compared to those treated with SAR405 **(Fig. 3D)**. This indicated that PI(3,4,5)P_3 was enriched at the plasma membrane and that it was

produced in a Vps34-dependent manner. A control set of cells were labeled with antibody alone. Only background fluorescence was observed demonstrating that CF488 fluorescence was Grp1-PH dependent.

To get a better sense of Vps34 activity in PI(3,4,5)P_3 production we used cells that expressed a temperature sensitive mutation of Vps34 (ts*vps34*). Cells were grown at the permissive temperature (30°C) or non-permissive temperatures (37°C) to modulate Vps34 activity without the need for chemical inhibitors. We found that inhibiting ts*vps34* reduced plasma membrane labeling with Grp1-PH, while labeling was preserved in cells grown at the permissive temperature **(Fig. 3E-F)**. Interestingly, vacuolar PI(3,4,5)P_3 staining was not observed in whole cells, which was likely due to the excess of plasma membrane content that masked the vacuolar signal. This was reminiscent of differential PI(4,5)P_2 staining between the plasma membrane and vacuoles. Plasma membrane PI(4,5)P_2 was in great excess preventing vacuole staining to be detected(Stefan et al., 2002). Vacuolar PI(4,5)P_2 was only detected when isolated from the cell (Mayer et al., 2000; Fratti et al., 2004).

To compare vacuolar versus whole cell PI(3,4,5)P_3 we extracted lipids and analyzed their concentration using a PI(3,4,5)P_3 mass ELISA kit (Choi et al., 2016; Gross et al., 2015). For vacuole measurements we extracted lipids from 3X fusion reactions (18 µg by protein) which contained approximately 3.5 pmol PI(3,4,5)P_3 **(Fig. 3G)**. The signal was abolished when vacuoles were treated with 150 nM PTEN prior to lipid extraction. Next, we extracted lipids from whole cells and found that whole cells contained 150 pmol PI(3,4,5)P_3, far more than vacuoles per µg of protein. Thus, it is not surprising that plasma membrane staining masked vacuole staining in whole cells. As a test for PTEN phosphatase activity, we used a malachite green assay to measure orthophosphate levels produced by PTEN activity on C8-PI(3,4,5)P_3 (Harmon et al., 2017). Reactions contained 300 nM GST-PTEN and 3 nM C8-PI(3,4,5)P_3 alone or in combination and incubated for 30 min at RT. This showed that our PTEN preparation was indeed active against C8-PI(3,4,5)P_3 **(Fig. 3H)**.

Blocking CF488-Grp1-PH labeling

Next, we tested if Grp1-PH labeling of vacuoles with active Vps34 could be eliminated or blocked. First, we treated vacuoles with PTEN prior to adding CF488-Grp1-PH and found that it sharply blocked labeling indicating that PI(3,4,5)P_3 was eliminated **(Fig. 4A-B)**. To confirm that this was not an indirect effect we next tested CF488-Grp1-PH localization by adding C8-PI(3,4,5)P_3 or C8-

PI(4,5)P_2 as competitive inhibitors. This showed that CF488-Grp1-PH labeling was inhibited by C8-PI(3,4,5)P_3 whereas C8-PI(4,5)P_2 had no effect **(Fig. 4C-D).** This further demonstrated that Grp1-PH labeling was PI(3,4,5)P_3-dependent.

PI(3,4,5)P_3 affected GFP-Ypt7 and HOPS enrichment at vertex domains

While examining vacuole docking with inhibitory levels of PTEN, Grp1-PH and C8-PI(3,4,5)P_3, we observed a reduction in the vacuole clusters as well the number of vacuoles per cluster. This suggested that PI(3,4,5)P_3 affected docking/tethering. To examine this, we used vacuoles containing GFP-Ypt7 and measured its enrichment at vertices when PI(3,4,5)P_3 was sequestered by Grp1-PH. This showed that sequestering PI(3,4,5)P_3 prevented GFP-Ypt7 enrichment at vertices **(Fig. 5A-B)**. GFP-Ypt7 was still visible on Grp1-PH treated vacuoles; however, the intensities at vertex sites were diminished while intensities at the outer edges were increased. To confirm that endogenous PI(3,4,5)P_3 availability affected GFP-Ypt7 distribution we used 250 μM C8-PI(3,4,5)P_3 as a competitive inhibitor. We found that adding C8-PI(3,4,5)P_3 also lead to the redistribution of GFP-Ypt7 throughout membranes **(Fig. 5C-D)**. These results demonstrated that PI(3,4,5)P_3 was needed for the assembly of vertex microdomains.

To see if other vertex components were affected by PI(3,4,5)P_3 we used vacuoles that contained Vps33-GFP, a HOPS subunit. Vps33-GFP localization to vertices has been shown to be sensitive to the lipid binding probes that target PI3P, PI(4,5)P_2, DAG and ergosterol (Fratti et al., 2004). Moreover, Vps33 can be released from vacuoles when PI3P, PI4P and PI(4,5)P_2 are sequestered (Stroupe et al., 2006). Here we tested the effects of C8-PI(3,4,5)P_3 and Grp1-PH on Vps33-GFP distribution. Untreated vacuoles contained enriched Vps33 at vertices as expected **(Fig. 5E-F)**. However, Vps33-GFP vertex enrichment was sharply reduced by C8-PI(3,4,5)P_3 and Grp1-PH, which further demonstrated that free PI(3,4,5)P_3 was required for normal vertex assembly.

PI(3,4,5)P_3 affects trans-SNARE pairing. While blocking or altering PI(3,4,5)P_3 affected the Ypt7-dependent tethering stage, the reduction did not account for the overall inhibition of fusion. Thus, it was likely that vertices that formed could be blocked after tethering. This was consistent with the gain of resistance experiments. The first known event downstream of tethering is the formation of trans-SNARE complexes between partner membranes. To examine trans-SNARE pairing we used two types of vacuoles. One type lacked the R-SNARE Nyv1 and expressed Vam3 with an internal calmodulin binding peptide between the N-terminal helical H_{abc} domain and the SNARE domain (CBP-*VAM3 nyv1*Δ). The second type contained Nyv1 and unmodified Vam3

(*VAM3 NVY1*) **(Fig. 6A)** (Collins and Wickner, 2007; Jun and Wickner, 2007). The formation of trans-SNARE complexes was detected when Nyv1 co-isolated with CBP-Vam3. We found that under control conditions CBP-Vam3 indeed paired with Nyv1 from partner membranes as well as the HOPS subunits Vps33 and Vps18 **(Fig. 6B-C)**. As a negative control we used NEM that inhibited SNARE priming and thus prevented downstream trans-SNARE interactions. As expected, NEM treatment abolished Nyv1 co-isolation with CBP-Vam3 but had no effect on Vam3-HOPS interactions **(Fig. 6B lane 7 vs 8)**.

To test the role of PI(3,4,5)P_3 in trans-SNARE pairing we used a curve of PTEN and found that it blocked CBP-Vam3 pairing with Nvy1. The block in trans-SNARE complex formation was likely to account for the incomplete inhibition of vertex assembly. The inhibition of trans-SNARE complex formation could be due to two factors. First, the Qb-SNARE Vti1 was absent from the CBP-Vam3 complex when PTEN at 200 nM even though it was present in the input **(Fig. 6B, lane 6 vs 12, and C)**. This is significant because the 3Q-SNAREs form stable complexes prior to binding Nyv1 in trans (Jun et al., 2006), suggesting that PI(3,4,5)P_3 affects SNAREs at more than one point. Second, Vam7 was depleted in the input membrane fraction and completely absent from CBP-Vam3 complexes when vacuoles were treated with 200 nM PTEN. It is important to note that the first step in trans-SNARE isolation is pelleting the membranes which separates vacuole-bound from unbound proteins. Thus, a release of Vam7 from the vacuole would result in its absence from the input blot. Together, this suggested that Vam7 was released from membranes when PI(3,4,5)P_3 was eliminated. Vam7 has been shown by others to bind PI(3,4,5)P_3 in lipid overlay assays (Yu and Lemmon, 2001). Consequently, it could be that Vam7 bound to PI(3,4,5)P_3 was needed for Vti1 to bind Vam3 in a 3Q-SNARE complex. We must note a previous study showed that Vti1-Vam3 binding is not affected by eliminating or blocking other PIs including PI3P, PI4P, and PI(4,5)P_2 (Collins and Wickner, 2007).

In addition to SNARE complex formation CBP-Vam3 also pulled down the HOPS complex. Surprisingly, when vacuoles were treated with PTEN we found that it did not inhibit HOPS co-isolating with CBP-Vam3. On the contrary, we discovered that depleting PI(3,4,5)P_3 enhanced HOPS binding to CBP-Vam3 **(Fig. 6B-C)**. Since tethering precedes docking, it is likely that this represents a pre-trans-SNARE Vam3-HOPS complex and that PI(3,4,5)P_3 leads to HOPS displacement to allow other SNAREs to interact with Vam3.

To confirm the effects of PTEN on trans-SNARE pairing we repeated the experiment using Grp1-PH. Grp1-PH showed a dose-dependent loss of Vam7 from the input lanes **(Fig. 6D, lanes 3-6)**, which was mirrored in pulldown efficiency **(Fig. 6D, lanes 9-12, and E)**. Similarly, there was a gradual loss in Nyv1 and Vti1 in the pulldown lanes but without their loss in the input. Considering that the 3Q-SNAREs are bound together in the presence of NEM, the effect of sequestering PI(3,4,5)P_3 suggests that the lipid is needed to stabilize the complex to promote optimal interactions with Nyv1. While not published, we must note that Vam3, Vti1 and Nyv1 all have polybasic regions (PBR) adjacent to their transmembrane domains (TMDs). A similar juxtamembrane PBR is present in Syntaxin1A that interacts with PI(3,4,5)P_3 to promote clustering and neurotransmitter release (Khuong et al., 2013). Apart from its effects on SNARE pairing, Grp1-PH also increased HOPS-Vam3 interactions as seen with PTEN **(Fig. 6D-E).**

Grp1-PH displaced Vam7 from membranes

To ask if the loss of Vam7 from vacuoles treated with PTEN and Grp1 was due to eliminating/sequestering PI(3,4,5)P_3 we tested protein binding in the presence of Grp1-PH. Fusion reactions were treated with buffer (0 μM) or GST-Grp1-PH at increasing concentrations. After incubation, vacuole-bound and unbound proteins were separated by centrifugation, and the two fractions were examined by immunoblotting. As seen previously, the soluble/peripheral proteins Vps18, Vps33, actin, and Vam7 were seen in both bound and unbound fractions **(Fig. 7A-B)**. In contrast, the membrane-anchored proteins Nyv1 and Ypt7 were only seen in the bound fraction. Treatment with GST-Grp1 only affected Vam7 binding where significantly more was released into the supernatant and depleted from the bound fraction **(Fig. 7A lanes 5 and 11)**. This was reminiscent of a previous study showing that Vam7 was released in the presence of the lipid binding domains FYVE, ENTH and C1b, which bind PI3P, PI(4,5)P_2 and DAG, respectively (Fratti et al., 2004). That said, HOPS binding was not meaningfully altered in the presence of Grp1-PH, whereas a previous study showed that Vps33 was significantly released by FYVE, ENTH as well as the PI4P binding domain Fapp1-PH (Stroupe et al., 2006). We also tested C8-PI(3,4,5)P_3 at 250 μM which inhibits fusion. Unlike Grp1-PH, C8-PI(3,4,5)P_3 had no effect on Vam7 binding. This could be due to differences in binding affinities where C8-PI(3,4,5)P_3 cannot compete with full length lipid. This also indicated that a separate factor required for fusion was blocked by C8-PI(3,4,5)P_3, which lead to the mislocalization of Ypt7 and Vps33. Together these data suggested that Vam7 release could be due to a direct interaction and not to a general blockage of vertex microdomain assembly/maintenance.

Vam7 binds PI(3,4,5)P_3

Vam7 uses its PX domain to bind the vacuole through its interactions with PI3P, and mutating Tyr42 to Ala blocks PI3P binding; however, Vam7^{Y42A} supports fusion albeit at a reduced level compared to the wild type (Boeddinghaus et al., 2002; Fratti and Wickner, 2007; Cheever et al., 2001). The ability of Vam7^{Y42A} to support fusion was attributed to its ability to interact with SNAREs and HOPS without the aid of PI3P. That said, it could be that Vam7^{Y42A} interacted with other lipids, including PI(3,4,5)P_3. Previously we showed that Vam7 also bound to PA and PI5P by liposome flotation, although binding affinities were not determined (Miner et al., 2016). We also observed weak PA binding by surface plasmon resonance, microscale thermophoresis and bio-layer interferometry (BLI) (Sparks et al., 2019, 2022; Calderin et al., 2025). This suggests that Vam7 could have a second lipid binding site or that its single site is promiscuous allowing multiple lipids to bind with variable affinities. The former is in accord a study showing that many PX domains have a second lipid binding site (Chandra et al., 2019).

Here we compared PI3P and PI(3,4,5)P_3 binding using streptavidin-coated biolayer interferometry (BLI) probes bound to biotinylated lipids. These were incubated with GST-Vam7 and GST-Vam7^{Y42A} at different concentrations to measure binding affinities. Here we show curves of response units versus protein concentration. This demonstrated that Vam7 bound to PI3P (K_D ≈200 nM) whereas Vam7^{Y42A} failed to bind as expected **(Fig. 7C)**. In comparison, we found that both Vam7 and Vam7^{Y42A} bound to PI(3,4,5)P_3 with K_D ≈70 and ≈210 nM, respectively **(Fig. 7D)**. Vam7 appeared to bind PI(3,4,5)P_3 with higher affinity versus PI3P. Could this indicate that a second site for PI(3,4,5)P_3 is preferred when the primary site for PI3P is inactive? The binding of Vam7^{Y42A} to PI(3,4,5)P_3 was also consistent with the notion that the PX domain could have a second binding site. Alternatively, other residues in the same binding pocket might have engaged the D4 and D5 phosphates of PI(3,4,5)P_3, which were not involved in binding with the D3 phosphate of PI3P. It was also possible that the Y42A mutation weakened PI(3,4,5)P_3 binding without abolishing it. Future investigation will explore these options.

Finally, we asked if Vam7 binding to b-PI(3,4,5)P_3 could be blocked. For this we used PIT-1 to inhibit PI(3,4,5)P_3-protein interactions. PIT-1 (200 μM) and Vam7 were pre-incubated together for then transferred to microtiter plate wells for BLI reactions. We found that PIT-1 abolished Vam7 binding to bPI(3,4,5)P_3 **(Fig. 7E).** This is in accord with the activity of PIT-1 on PI(3,4,5)P_3 interactions with lipid binding domains.

Discussion

In this study we asked if there was a role for PI(3,4,5)P_3 in yeast vacuole fusion. We showed that C8-PI(3,4,5)P_3 inhibited fusion at time between the GDI-sensitive/Ypt7-dependent step and trans-SNARE pairing. Separately we found that sequestering endogenous PI(3,4,5)P_3 with Grp1-PH or modifying it with PTEN inhibited fusion. Furthermore, blocking PI(3,4,5)P_3 interactions with PIT-1 and DMPIT rescued inhibition by Grp1 and PTEN. Together these data indicate that vacuoles contain PI(3,4,5)P_3 and that it interacts with a least one vacuolar protein to promote optimal fusion.

Importantly, experiments using SAR405 and the ts*vps34* mutation showed that baker's yeast produces PI(3,4,5)P_3 at the plasma membrane and vacuolar compartments. Thus, we conclude that PI(3,4,5)P_3 is made by Vps34 using PI(4,5)P_2 as a substrate. This was shown in *Schizosaccharomyces pombe* by others (Mitra et al., 2004). While more convoluted pathways could be drawn to link Vps34 and PI(3,4,5)P_2, it is more likely that the more direct pathway of adding a third phosphate to PI(4,5)P_2 was used. This supports the idea that PI(3,4,5)P_3 production was established prior to the evolutionary rise of other PI 3-kinases.

Vam7 and vertex microdomains

Stage specific experiments showed that both Ypt7-dependent tethering and trans-SNARE pairing required PI(3,4,5)P_3. The Ypt7-dependent effect was shown by the lack of its enrichment at vertices. Docked vacuoles form vertex microdomains that become enriched in Ypt7, HOPS, SNAREs and actin, as well as PI3P, PI(4,5)P_2, DAG, and ergosterol (Wang et al., 2002, 2003; Eitzen et al., 2002; Karunakaran et al., 2012; Fratti et al., 2004). The composition of the vertices is highly regulated, and interdependent and their correct organization promotes trans-SNARE pairing and fusion.

Vam7 and PI(3,4,5)P_3

The interaction between Vam7 and PI3P has long been recognized as the mechanism by which it associates with membranes prior to its interactions with its cognate SNAREs and HOPS (Cheever et al., 2001; Boeddinghaus et al., 2002). Its lipid binding capacity lies in its N-terminal PX domain and PI3P binding can be largely abolished by mutating Tyr42 to Ala. That said, Vam7^{Y42A} can still associate with vacuoles and support fusion at reduced levels (Fratti and Wickner, 2007). This was attributed to its interactions with proteins and not other lipids. Here we showed that Vam7 and Vam7^{Y42A} can both bind to b-PI(3,4,5)P_3 by BLI implying that a second

binding site exits as seen in other PX domains (Chandra et al., 2019). An alternative explanation could lie in the use of additional residues in the same PI3P-binding pocket to accommodate PI(3,4,5)P_3 binding that are not involved in PI3P binding. Thus, mutating Tyr42 to Ala blocked PI3P binding with little effect on PI(3,4,5)P_3 binding.

Although Vam7 strongly bound to PI(3,4,5)P_3 we showed that it can be released from vacuoles when native PI(3,4,5)P_3 is blocked Grp1-PH or modified with PTEN in the presence of PI3P. This poses the question: Why are two lipid interactions are needed? PI3P is delivered to vacuoles via endolysosomal trafficking in low concentrations and the pool of PI3P is regenerated by a new round of production on site (Thorngren et al., 2004). It is possible that the ebb and flow of PI3P levels could negatively impact Vam7 recruitment to vacuoles and that a second ligand is needed for stable association with the membrane. Originally, we hypothesized that PA could be the initial binding partner and that its conversion to DAG by Pah1 would lead to a hand off to PI3P. This was based on the required conversion of PA to DAG during pre-priming and the idea that Vam7 only binds one lipid at a time (Sasser et al., 2012; Starr et al., 2019, 2016). Now we must consider that PI(3,4,5)P_3 could be the binding initiator, and that Vam7 could bind two lipids simultaneously.

Another question to consider is whether Vam7-PI(3,4,5)P_3 interactions affect Ypt7 and HOPS enrichment at vertex microdomains. It could be that changes in Vam7 conformation induced by PI(3,4,5)P_3 binding influences how HOPS interacts with Ypt7. This is not unlikely as both Vam7 and Ytp7 interact with the HOPS complex although not necessarily at the same time as seen by pulldown experiments (Price et al., 2000a; Seals et al., 2000; Brett et al., 2008; Stroupe et al., 2006; Collins et al., 2005; Fratti and Wickner, 2007; Fratti et al., 2007). A more direct effect would be through disrupting Vam7-Ypt7 binding. A yeast-two-hybrid screen showed that Vam7 and Ypt7 interact directly (Uetz et al., 2000). However, this scenario is less likely as the screen did not include PI(3,4,5)P_3. Furthermore, Vam7 pulldowns have failed to show Ypt7 (Stroupe et al., 2006).

Finally, how does PI(3,4,5)P_3 affect 3Q-SNARE complex formation? Our data showed that PTEN and Grp1-PH led to the exclusion of Vti1 and Vam7 from CBP-Vam3 complexes. The absence of Vam7 is attributed to its release from the membrane, but Vti1 has a TMD and was not displaced from vacuoles. Interestingly, the hydrophilic helical region adjacent to the Vti1 TMD has a PBR with 5 Lys and Arg that could participate in binding negatively charged lipids including PI(3,4,5)P_3, however this remains to be tested. Other SNAREs including Syntaxin-1 and Syntaxin-17 have TMD-adjacent PBRs that bind to PIPs to promote function in chromaffin granule secretion and

autophagy, respectively (Laczkó-Dobos et al., 2024; Lam et al., 2008). Future studies will test whether the Vti1 PBR promotes binding to Vam3 followed by Vam7, if Vam7 binds Vam3 before Vti1, or if complex formation is concurrent.

In conclusion, this study has shown that PI(3,4,5)P_3 is critical in the regulation of vacuole homotypic fusion at multiple steps. While this study ends at the trans-SNARE complex stage, the gain of resistance data suggest that additional down-stream stages could be affected by PI(3,4,5)P_3. Beyond vacuole fusion it is likely that PI(3,4,5)P_3 signals through the yeast homologs of PDK1 (Pkh1/2), AKT1 (Sch9), PKC (Pkc1) and MAPK (Fus1, Kss1, Mpk1) to influence other functions such as autophagy, Ca^{2+} transport, and actin remodeling (Brady et al., 2006; Inagaki et al., 1999; Ni et al., 2013; Levina et al., 2022; Asano et al., 2008; Dieterle et al., 2014; Kassouf et al., 2015; Hsu et al., 2000).

Materials and methods

Reagents

Reagents were solubilized in PIPES-Sorbitol (PS) buffer (20 mM PIPES-KOH, pH 6.8, 200 mM sorbitol) with 125 mM KCl unless indicated otherwise. PIPES [Piperazine-N-N'-bis(2-ethanesulfonic acid)], HEPES [N-(2-Hydroxyethyl)piperazine-N′-(2-ethanesulfonic acid)], NEM (N-ethylmaleimide), Coenzyme A (CoA), Creatine kinase, and reduced glutathione were purchased from Sigma (St. Louis, MO) and dissolved in PS buffer or DMSO. Sorbitol, ATP, Yeast extract, Tryptone, Glucose Tris base, Triton X100 and DTT were purchased from RPI (Mount Prospect, IL). FM4-64, Goat anti-rabbit IgG (H+L) secondary antibody DyLight 650 conjugate, Fluoromount-G with DAPI, glycerol, and glutathione agarose were from Thermo-Fisher (Waltham, MA). Fluorescent CF488 goat-anti GST was from Biotium (Fremont, CA). Poly-L-Lysine was from Santa Criz Biotechnology (Dallas, TX). Creatine phosphate was from Abcam (Waltham, MA). PIT-1, 3,5-dimethyl PIT-1 (DMPIT), and SAR405 were from Cayman Chemical and dissolved in DMSO (Ann Arbor, MI). C8-PC (1,2-dioctanoyl-sn-glycero-3-phosphatidylcholine), C8-PE (1,2-dioctanoyl-sn-glycero-3-phosphatidylethanolamine), C8-PS (1,2-dioctanoyl-sn-glycero-3-phosphatidylserine) were from Avanti (Alabaster, AL). C8-PI3P (1,2-dioctanoyl-sn-glycero-3-phosphatidylinositol 3-phosphate), C8-PI(3,5)P_2, C8-PI(4,5)P_2, C8-PI(3,4,5)P_3, biotin-PI3P (b-PI3P), b-PI(3,4,5)P_3, Inositol-1,3,4-trisphosphate (Ins(1,3,4)P_3), Inositol-1,3,5-trisphosphate (Ins(1,3,5)P_3), Inositol-1,3,4,5-tetraphosphate (Ins(1,3,4,5)P_4), the PI(3,4,5)P_3 mass ELISA kit and the malachite green phosphatase kit were from Echelon (Salt Lake City UT). *p*-nitrophenyl

phosphate was from MP Biomedicals (Santa Ana, Ca). Calmodulin agarose was Agilent (Santa Clara, CA). Octet Streptavidin (SA) biosensors were from Sartorius (Göttingen, Germany). Nitrocellulose was from BioRad (Hercules, CA).

Plasmids and Recombinant proteins

Recombinant GST-Vam7, GST-Vam7^{Y42A}, GDI, Pbi2 (Inhibitor of proteinase B) and Oxylyticase were prepared as described previously (Fratti and Wickner, 2007; Miner et al., 2016; Fratti et al., 2007; Starai et al., 2007; Slusarewicz et al., 1997; Scott and Schekman, 1980). Plasmids to produce GST-Grp1-PH and GST-PTEN, were from Addgene (Watertown, MA). The plasmid to make GST-Grp1-PH^{K273A} was a gift from Dr. N. Leslie (Heriot Watt University, Edinburgh, UK) (Lindsay et al., 2006). Plasmids were transformed into *E. coli* BL21 DE3 pLysS (New England Biolabs) and induced with 0.1 μM IPTG for 16h at 18°C. GST-tagged proteins were isolated using standard methods with glutathione agarose, eluted with reduced glutathione and dialyzed against PS buffer (20 mM PIPES-KOH pH 6.8, 200 mM sorbitol, 125 mM KCl, 5 mM $MgCl_2$) with 125 mM KCl.

Strains, Vacuole isolation and fusion

Yeast strains were grown in YPD (1% yeast extract, 2% peptone, 2% dextrorse) or synthetic drop-out media without Trp or Ura. The pH of drop out media was adjusted to 6.0. The temperature sensitive *VPS34* mutant (ts*vps34*) was a gift from Dr. D. Klionsky (University of Michigan). Vacuoles were isolated as described (Haas et al., 1994). *In vitro* fusion reactions (30 μl) contained 3 μg each of vacuoles from BJ3505 (*PHO8 pep4*Δ) and DKY6281 (*pho8*Δ *PEP4*) backgrounds, reaction buffer (20 mM PIPES-KOH pH 6.8, 200 mM sorbitol, 125 mM KCl, 5 mM $MgCl_2$), ATP regenerating system (1 mM ATP, 0.1 mg/ml creatine kinase, 29 mM creatine phosphate), 10 μM CoA, and 283 nM Pbi2 (Protease B inhibitor) (Jones et al., 1982; Klionsky and Emr, 1989). Fusion was determined by the processing of pro-Pho8 (alkaline phosphatase) from BJ3505 by the Pep4 protease from DK6281. Fusion reactions were incubated at 27°C for 90 min and Pho8 activity was measured in developer solution (250 mM Tris-HCl pH 8.5, 0.4% Triton X-100, 10 mM $MgCl_2$, and 1 mM *p*-nitrophenyl phosphate). Pho8 activity was stopped after 5 min by addition of 1 M glycine pH 11 and fusion units were measured by determining the *p*-nitrophenolate produced by absorbance at 400 nm.

Trans-SNARE complex isolation

Trans-SNARE pairing was measured as previously described with some modifications (Collins and Wickner, 2007; Jun et al., 2007; Qiu and Fratti, 2010; Sasser et al., 2012, 2013). Large scale 15X (450 µL) fusion reactions containing 45 µg of DKY6281 vacuoles (*VAM3 NYV1*) and 45 µg of BJ3505 vacuoles that lacked *NYV1* and contained Vam3 tagged with an internal calmodulin binding peptide (CBP) between the H_{abc} and SNARE domains (*CBP-VAM3 nyv1*Δ) (Collins and Wickner, 2007). Reactions were treated with buffer alone or 2 mM NEM as a negative control to prevent SNARE activation. Separate reactions were treated with GST-PTEN or GST-Grp1-PH at the indicated concentrations. Reactions were incubated for 60 min at 27°C then placed on ice for 5 min before centrifugation (13,000 g, 15 min, 4°C) to pellet membranes. The supernatants were carefully removed, and the pellets were overlaid and resuspended with 200 µL cold solubilization buffer (SB: 20 mM Tris-Cl, pH 7.5, 150 mM NaCl, 1 mM $MgCl_2$, 0.5% Nonidet P-40 alternative, 10% glycerol) with protease inhibitors (1 mM PMSF and 1 complete™ protease inhibitor tablet per 10 ml SB). Reactions were brought up to 600 µL with additional SB and nutated at 4°C for 20 min. Insoluble debris was removed by centrifugation (16,000 g, 20 min, 4°C). Solubilized (580 µL) material was transferred to pre-chilled tubes and 58 µL was removed from each reaction as 10% of the total reactions. $CaCl_2$ was added to each sample to a final concentration of 2 mM. Next, 50 µL of calmodulin beads equilibrated with SB was added to each reaction. Mixtures were nutated overnight at 4°C. CBP-Vam3 complexes bound material was collected by centrifugation (1,300 x g, 2 min, 4°C) and washed 4 times with 600 µL fresh ice-cold SB. Calmodulin bound material was eluted with 1X SDS loading buffer containing 5 mM EGTA and boiled for 5 min. Samples were resolved by SDS-PAGE, transferred to nitrocellulose and probed with antibodies against Vam3, Vam7, Nyv1, Vti1, Vps33 and Vps18. Bound primary antibodies were visualized with DyLight 650-Goat anti-rabbit IgG (H+L).

Fluorescence microscopy of vacuoles and vertex microdomain formation

Isolated vacuoles from BJ3505 or from cells expressing GFP-Ypt7 or Vps33-GFP were subjected to docking assays as previously described (Fratti et al., 2004; Wang et al., 2002) with slight modifications. Reactions (30 µL) contained 6 µg of vacuoles isolated from the indicated strains in fusion reaction buffer modified for docking conditions (PS buffer, 100 mM KCl, 0.5 mM $MgCl_2$, 0.33 mM ATP, 13 mM creatine phosphate, 33 µg/mL creatine kinase, 10 µM coenzyme A, and 280 nM IB_2). Measuring the vertex enrichment of factors during tethering and docking was performed with vacuoles from cells expressing GFP fusion proteins or labeled with lipid binding probes. To track GFP-Ypt7 and Vps33 localization reactions were incubated under docking

conditions as described above and stained with 4 μM FM4-64 prior to examination(Wang et al., 2003; Fratti et al., 2004). To localize the distribution of PI(3,4,5)P_3 on vacuoles, reactions were incubated with 150 nM GST-Grp1-PH. GST was then visualized with fluorescent (CF488) goat-anti-GST antibody. Briefly, reactions were treated with PS buffer, DMSO, PTEN or SAR405 for 5 min, followed by adding 150 nM GST-Grp1-PH and incubating for 5 min. Next, CF488-anti-GST antibody was added to each reaction and further incubated for 20 min. Following incubation, reactions were gently centrifuged to remove unbound material, resuspended with PS buffer and mixed with 20 μL of 0.6% low melt agarose in PS buffer melted at 50°C and cooled to prior to mixing with vacuoles. Next, 20 μL aliquots were mounted on pre-chilled slides and observed by fluorescence microscopy. Images were acquired using a Zeiss Axio Observer Z1 inverted microscope equipped with an X-Cite 120XL light source, Plan Apochromat 63X oil objective (NA 1.4), and an AxioCam CCD camera. CF488 was visualized using a 38 HE EGFP shift-free filter set and FM4-64 was visualized with a 42 HE CY 3 shift-free filter set. Exposure times were set using WT vacuoles for each fluorescence channel and scripts acquired non-specific images followed by specific reporters. This ensures that bleaching is consistent to negate it as a factor in calculating intensity ratios. Exposure times were held constant within an experiment.

Images were analyzed using ImageJ software (NIH). Vertex enrichment was determined by first measuring maximum fluorescence intensity in each channel at each contact point between membranes, *i.e.*, vertex domain within a cluster. Next, fluorescence intensity was measured in each channel at outer membrane domains where vacuoles are not in contact with other membranes. The ratio of specific (*e.g.,* GFP) to non-specific (*e.g.,* FM4-64) was determined for vertices and outer membrane domains and compared for relative enrichment. Measurements for each condition were taken of 15-20 clusters to yield 100-300 vertices for each condition/strain per experiment. Data from multiple experiments were combined in column plots showing individual values as well as the geometric means and geometric standard deviation for each condition.

Fluorescence microscopy of whole cells

BJ3505 or Sey6210 ts*vps34* cells were inoculated in YPD or complete synthetic medium without Uracil and grown overnight at 30°. Cultures were diluted to 0.25 OD_{600} into 10 ml of fresh YPD incubated until OD600 reached 0.4-0.6 at 30°C or 37°C. Cells were fixed with 3.7% Formaldehyde for 60 min. Fixed cells pellets were collected and washed twice with 1 ml 1X PBS buffer and resuspended in 0.5 ml spheroplast buffer (50 mM KPi buffer pH 7.5, 600 mM Sorbitol, 0.2% YPD). Cell suspensions (200 μL) were mixed with 70 μg oxalyticase and 0.5 μL stock 2-mercaptoethanol

and incubated in a 30°C water bath for 60-90 min. Cells were then washed once with 1 ml of 1X PBS + 0.05% Tween 20 and resuspended in 50 µl of PBS + 0.05% Tween 20 then 40 µl of cells were transferred onto coverslips coated with 0.1% Poly-L-lysine in a 6-well dish and incubated on a shaker at room temperature for 5-10 minutes. After incubation, the fluid was aspirated the coverslips were washed 3 times with 1 mL 1X PBS buffer to ensure that the coverslips remained submerged during each wash. Coverslips were dried and cells were blocked with PBS + 1mg/ml BSA for 30 min at room temperature, then washed 3 times with 1X PBS buffer. Next, a 10 µM GST-Grp1-PH solution diluted with PBS with 1mg/ml BSA was added to coverslips and incubated for 1 h at room temperature. After incubation, the coverslips were washed 3 times with 1X PBS buffer and incubate with 1:5000 CF-488 anti-GST fluorescent antibody diluted in PBS + 1mg/ml BSA in the dark for 30 min. Coverslips are washed 3 more times with 1X PBS buffer and are dried for a few minutes before mounting onto pre-cleaned microscope slides with 10 µl mounting media (fluoromount-G™ with DAPI) followed by imaging by fluorescence microscopy.

Images were analyzed using ImageJ software (NIH). Maximum fluorescence intensities were measured using a DAPI filter or a GFP filter set for CF488. The ratio of CF488-Grp1-PH (PI(3,4,5)P_3) to DAPI was determined for each cell. Measurements for each condition were taken of ~100 cells per condition per experiment. Data from multiple experiments were combined in column plots showing individual values as well as the geometric means and geometric standard deviation for each condition.

Immunoblotting

Vacuoles were solubilized with 95°C 1-5X Laemmli buffer for 5 min. Extracts were resolved using 10% SDS-PAGE and transferred to nitrocellulose for immunoblotting. Rabbit antibodies against Actin, Nyv1, Vam3, Vps18, Vps33 and Ypt7 were prepared as described (Eitzen et al., 2002; Nichols et al., 1997; Seals et al., 2000; Haas et al., 1995). Goat anti-rabbit IgG (H+L) antibody DyLight 650 conjugate was used as a secondary antibody. Fluorescence was measured with an Azure 400.

Bio-Layer Interferometry (BLI)

Vam7 binding to lipids was measured by BLI as described (Calderin et al., 2025). Biotinylated PI3P and PI(3,4,5)P_3 were resuspended in PS buffer to a final stock concentration of 0.1 mM. Lipids were diluted to 500 nM with BLI running buffer (PBS with 0.002% Tween-20, v/v) and 190 µL was added to wells in a 96-well microplate. GST-Vam7, and GST-Vam7^{Y42A} was diluted to 100,

200, 400, and 800 nM with BLI running buffer and 190 µL of each dilution, for each analyte, were loaded to corresponding wells.

Lipid extraction for PI(3,4,5)P_3 ELISA

Yeast vacuoles were isolated and collected as stated above and prepared for fusion conditions without Pbi2 and ATP regeneration system. Instead, we used 2 mM ATP/$MgCl_2$ and incubated for 90 min. Lipids were extracted as described with some modification (Hsu et al., 2000). After the incubation, 300 µL of chilled acetone was added to each reaction on ice for 5 min. Reaction volumes were split 50:50 into two 2 mL tubes containing 1.5 mL MeOH/CHCl3 (1:1) and vortexed heavily at RT followed by centrifugation (3,000 g, 5 min at 4°C). The supernatants were carefully discarded, and the remaining pellets were resuspended with 1.25 mL MeOH:$CHCl_3$:HCl (80:40:1) and vortexed at RT until the pellets were dispersed in solution (~5 min). Suspensions were transferred to new 15 mL conical tubes after which 750 µL $CHCl_3$ and 1.35 mL 0.1 M HCl were added to each tube. Extracts were then vortexed and centrifuged (3,000 g, 5-10 min). The lower phases (1.5 mL) were carefully transferred to 1.5 mL microcentrifuge tubes and dried in a speed vac or under a N_2 stream. The lipid films were resuspended in 10 µL $CHCl_3$. Endogenous vacuolar PI(3,4,5)P_3 levels were measured using as ELISA kit following the manufacturers' instructions as shown elsewhere (Gross et al., 2015; Costa et al., 2015).

For whole cell analysis, BJ3505 cells were grown to an average OD_{600} of 0.7 and prepared for spheroplasting treatment as mentioned above for yeast vacuole isolation. Following incubation, the cells were pelleted (3,000 g, 5-10 min). Supernatants were removed, and the corresponding cell pellets were resuspended in 100 µL of PS Buffer. Pellets were resuspended in 50 µL in PS buffer and added to fusion conditions as mentioned above and incubated for 90 minutes. Lipids were then extracted following the same protocol for vacuoles.

Phosphatase activity assay

A malachite green phosphatase assay was used to detect PTEN activity. Reactions (50 µL) in 96-well plates contained 300 nM GST-PTEN, 3 nM C8-PI(3,4,5)P_3 alone or in combination. Next, 10 µL of reagent A (42.8 mM Na_2MoO_4, 1.14 M HCL) was added to each well and incubated for 10 min at room temperature. After the incubation, 10 µL or Reagent B (0.042% w/v malachite green, 1% w/v polyvinyl alcohol) was added to each well and incubated for an additional 20 min at RT. Reactions were stopped with 10 µL 7.8% H_2SO_4 and free orthophosphate was measured at 630 nm. Concentrations were derived using a Pi standard curve.

Quantification and statistical analysis

Fusion results were expressed as the mean ± SEM or geometric mean ± SD as needed. Experimental replicates (n) are defined as the number of separate experiments. For comparison of vertex enrichment all the ratio data was log-transformed to yield near-normal distribution with comparable variances. Non-parametric analysis gave indistinguishable results. Statistical analysis was performed by unpaired two-tailed t-test or One-Way ANOVA for multiple comparisons using Prism 10 (GraphPad, San Diego, CA). Statistical significance is represented as follows: *p<0.05, **p<0.01, ***p<0.001, ****p<0.0001. Tukey, Dunnett, and Šidák post hoc tests were used for multiple comparisons and individual p-values.

Data availability

All data generated or analyzed during this study are available upon request. Addition data sharing information is not applicable to this study.

Acknowledgements

The authors wish to thank Dr. William Wickner for the generous gifts of antibodies. Dr. Nicholas Leslie for donated plasmids and Dr. Daniel Klionsky for the tsVPS34 strain. This research was supported by a grant from the National Science Foundation (MCB 2216742) to RAF. JDC was partially supported by an NIGMS-NIH Chemistry-Biology Interface Training Grant (5T32-GM070421).

Author contributions

Conceptualization: C.Z., J.D.C. and R.A.F.; Data curation: C.Z., J.D.C. and R.A.F.; Formal analysis: C.Z., J.D.C. and R.A.F.; Investigation: C.Z., J.D.C., A.T., V.S., J.M.K., C.K., R.A., D.G., E.W. and R.A.F.; Methodology: C.Z., J.D.C. and R.A.F.; Visualization: R.A.F.; Writing-original draft: C.Z., J.D.C. and R.A.F.; Writing-review and editing: All authors; Resources: R.A.F.; Supervision: R.A.F.; Project administration: R.A.F.; Funding acquisition: R.A.F.

Conflict of interest

The authors declare that they have no conflict of interest.

References

Asano, Y., A. Nagasaki, and T.Q.P. Uyeda. 2008. Correlated waves of actin filaments and PIP3 in Dictyostelium cells. *Cell Motil. Cytoskeleton*. 65:923–934. doi:10.1002/cm.20314.

Balla, T. 2013. Phosphoinositides: Tiny Lipids With Giant Impact on Cell Regulation. *Physiol. Rev.* 93:1019–1137. doi:10.1152/physrev.00028.2012.

Boeddinghaus, C., A.J. Merz, R. Laage, and C. Ungermann. 2002. A cycle of Vam7p release from and PtdIns 3-P-dependent rebinding to the yeast vacuole is required for homotypic vacuole fusion. *J. Cell Biol.* 157:79–89. doi:10.1083/jcb.200112098.

Bonangelino, C.J., J.J. Nau, J.E. Duex, M. Brinkman, A.E. Wurmser, J.D. Gary, S.D. Emr, and L.S. Weisman. 2002. Osmotic stress-induced increase of phosphatidylinositol 3,5-bisphosphate requires Vac14p, an activator of the lipid kinase Fab1p. *J. Cell Biol.* 156:1015–1028. doi:10.1083/jcb.200201002.

Brady, J.D., E.D. Rich, J.R. Martens, J.W. Karpen, M.D. Varnum, and R.L. Brown. 2006. Interplay between PIP3 and calmodulin regulation of olfactory cyclic nucleotide-gated channels. *Proc. Natl. Acad. Sci.* 103:15635–15640. doi:10.1073/pnas.0603344103.

Brett, C.L., R.L. Plemel, B.T. Lobingier, B.T. Lobinger, M. Vignali, S. Fields, and A.J. Merz. 2008. Efficient termination of vacuolar Rab GTPase signaling requires coordinated action by a GAP and a protein kinase. *J. Cell Biol.* 182:1141–1151. doi:10.1083/jcb.200801001.

Cabrera, M., M. Nordmann, A. Perz, D. Schmedt, A. Gerondopoulos, F. Barr, J. Piehler, S. Engelbrecht-Vandré, and C. Ungermann. 2014. The Mon1-Ccz1 GEF activates the Rab7 GTPase Ypt7 via a longin-fold-Rab interface and association with PI3P-positive membranes. *J. Cell Sci.* 127:1043–1051. doi:10.1242/jcs.140921.

Calderin, J.D., C. Zhang, T.J.C. Tan, N.C. Wu, and R. Fratti. 2025. Use of Bio-Layer Interferometry (BLI) to Measure Binding Affinities of SNAREs and Phosphoinositides. *Methods Mol. Biol. Clifton NJ*. 2887:103–117. doi:10.1007/978-1-0716-4314-3_7.

Chandra, M., Y.K.-Y. Chin, C. Mas, J.R. Feathers, B. Paul, S. Datta, K.-E. Chen, X. Jia, Z. Yang, S.J. Norwood, B. Mohanty, A. Bugarcic, R.D. Teasdale, W.M. Henne, M. Mobli, and B.M. Collins. 2019. Classification of the human phox homology (PX) domains based on their phosphoinositide binding specificities. *Nat. Commun.* 10:1528. doi:10.1038/s41467-019-09355-y.

Cheever, M.L., T.K. Sato, T. de Beer, T.G. Kutateladze, S.D. Emr, and M. Overduin. 2001. Phox domain interaction with PtdIns(3)P targets the Vam7 t-SNARE to vacuole membranes. *Nat. Cell Biol.* 3:613–618. doi:10.1038/35083000.

Chen, H.-C., B.P. Ziemba, K.E. Landgraf, J.A. Corbin, and J.J. Falke. 2012. Membrane Docking Geometry of GRP1 PH Domain Bound to a Target Lipid Bilayer: An EPR Site-Directed Spin-Labeling and Relaxation Study. *PLOS ONE*. 7:e33640. doi:10.1371/journal.pone.0033640.

Choi, S., A.C. Hedman, S. Sayedyahossein, N. Thapa, D.B. Sacks, and R.A. Anderson. 2016. Agonist-stimulated phosphatidylinositol-3,4,5-trisphosphate generation by scaffolded phosphoinositide kinases. *Nat. Cell Biol.* 18:1324–1335. doi:10.1038/ncb3441.

Collins, K.M., N.L. Thorngren, R.A. Fratti, and W.T. Wickner. 2005. Sec17p and HOPS, in distinct SNARE complexes, mediate SNARE complex disruption or assembly for fusion. *EMBO J.* 24:1775–1786. doi:10.1038/sj.emboj.7600658.

Collins, K.M., and W.T. Wickner. 2007. Trans-SNARE complex assembly and yeast vacuole membrane fusion. *Proc. Natl. Acad. Sci. U. S. A.* 104:8755–8760. doi:10.1073/pnas.0702290104.

Corbin, J.A., R.A. Dirkx, and J.J. Falke. 2004. GRP1 Pleckstrin Homology Domain: Activation Parameters and Novel Search Mechanism for Rare Target Lipid. *Biochemistry*. 43:16161–16173. doi:10.1021/bi049017a.

Corvera, S., A. D'Arrigo, and H. Stenmark. 1999. Phosphoinositides in membrane traffic. *Curr. Opin. Cell Biol.* 11:460–465. doi:10.1016/S0955-0674(99)80066-0.

Costa, C., H. Ebi, M. Martini, S.A. Beausoleil, A.C. Faber, C.T. Jakubik, A. Huang, Y. Wang, M. Nishtala, B. Hall, K. Rikova, J. Zhao, E. Hirsch, C.H. Benes, and J.A. Engelman. 2015. Measurement of PIP3 Levels Reveals an Unexpected Role for p110β in Early Adaptive Responses to p110α-Specific Inhibitors in Luminal Breast Cancer. *Cancer Cell*. 27:97–108. doi:10.1016/j.ccell.2014.11.007.

Cronin, T.C., J.P. DiNitto, M.P. Czech, and D.G. Lambright. 2004. Structural determinants of phosphoinositide selectivity in splice variants of Grp1 family PH domains. *EMBO J.* 23:3711–3720. doi:10.1038/sj.emboj.7600388.

Dieterle, A.M., P. Böhler, H. Keppeler, S. Alers, N. Berleth, S. Drießen, N. Hieke, S. Pietkiewicz, A.S. Löffler, C. Peter, A. Gray, N.R. Leslie, H. Shinohara, T. Kurosaki, M. Engelke, J. Wienands, M. Bonin, S. Wesselborg, and B. Stork. 2014. PDK1 controls upstream PI3K expression and PIP3 generation. *Oncogene*. 33:3043–3053. doi:10.1038/onc.2013.266.

Dowler, S., R.A. Currie, D.G. Campbell, M. Deak, G. Kular, C.P. Downes, and D.R. Alessi. 2000. Identification of pleckstrin-homology-domain-containing proteins with novel phosphoinositide-binding specificities. *Biochem. J.* 351:19–31. doi:10.1042/0264-6021:3510019.

Dunn, R., D.A. Klos, A.S. Adler, and L. Hicke. 2004. The C2 domain of the Rsp5 ubiquitin ligase binds membrane phosphoinositides and directs ubiquitination of endosomal cargo. *J. Cell Biol.* 165:135–144. doi:10.1083/jcb.200309026.

Eitzen, G., L. Wang, N. Thorngren, and W. Wickner. 2002. Remodeling of organelle-bound actin is required for yeast vacuole fusion. *J. Cell Biol.* 158:669–679. doi:10.1083/jcb.200204089.

Ferguson, K.M., J.M. Kavran, V.G. Sankaran, E. Fournier, S.J. Isakoff, E.Y. Skolnik, and M.A. Lemmon. 2000. Structural Basis for Discrimination of 3-Phosphoinositides by Pleckstrin Homology Domains. *Mol. Cell*. 6:373–384. doi:10.1016/S1097-2765(00)00037-X.

Fields, I.C., S.M. King, E. Shteyn, R.S. Kang, and H. Fölsch. 2010. Phosphatidylinositol 3,4,5-trisphosphate localization in recycling endosomes is necessary for AP-1B-dependent sorting in polarized epithelial cells. *Mol. Biol. Cell*. 21:95–105. doi:10.1091/mbc.e09-01-0036.

Fratti, R.A., K.M. Collins, C.M. Hickey, and W. Wickner. 2007. Stringent 3Q.1R composition of the SNARE 0-layer can be bypassed for fusion by compensatory SNARE mutation or by lipid bilayer modification. *J. Biol. Chem.* 282:14861–14867. doi:10.1074/jbc.M700971200.

Fratti, R.A., Y. Jun, A.J. Merz, N. Margolis, and W. Wickner. 2004. Interdependent assembly of specific regulatory lipids and membrane fusion proteins into the vertex ring domain of docked vacuoles. *J. Cell Biol.* 167:1087–1098. doi:10.1083/jcb.200409068.

Fratti, R.A., and W. Wickner. 2007. Distinct targeting and fusion functions of the PX and SNARE domains of yeast vacuolar Vam7p. *J. Biol. Chem.* 282:13133–13138. doi:10.1074/jbc.M700584200.

Gallego, O., M.J. Betts, J. Gvozdenovic-Jeremic, K. Maeda, C. Matetzki, C. Aguilar-Gurrieri, P. Beltran-Alvarez, S. Bonn, C. Fernández-Tornero, L.J. Jensen, M. Kuhn, J. Trott, V. Rybin, C.W. Müller, P. Bork, M. Kaksonen, R.B. Russell, and A.-C. Gavin. 2010. A systematic screen for protein-lipid interactions in Saccharomyces cerevisiae. *Mol. Syst. Biol.* 6:430. doi:10.1038/msb.2010.87.

Gross, C., C.-W. Chang, S.M. Kelly, A. Bhattacharya, S.M.J. McBride, S.W. Danielson, M.Q. Jiang, C.B. Chan, K. Ye, J.R. Gibson, E. Klann, T.A. Jongens, K.H. Moberg, K.M. Huber, and G.J. Bassell. 2015. Increased Expression of the PI3K Enhancer PIKE Mediates Deficits in Synaptic Plasticity and Behavior in Fragile X Syndrome. *Cell Rep.* 11:727–736. doi:10.1016/j.celrep.2015.03.060.

Guillou, H., C. Lécureuil, K.E. Anderson, S. Suire, G.J. Ferguson, C.D. Ellson, A. Gray, N. Divecha, P.T. Hawkins, and L.R. Stephens. 2007. Use of the GRP1 PH domain as a tool to measure the relative levels of PtdIns(3,4,5)P3 through a protein-lipid overlay approach. *J. Lipid Res.* 48:726–732. doi:10.1194/jlr.D600038-JLR200.

Haas, A., B. Conradt, and W. Wickner. 1994. G-protein ligands inhibit in vitro reactions of vacuole inheritance. *J. Cell Biol.* 126:87–97. doi:10.1083/jcb.126.1.87.

Haas, A., D. Scheglmann, T. Lazar, D. Gallwitz, and W. Wickner. 1995. The GTPase Ypt7p of Saccharomyces cerevisiae is required on both partner vacuoles for the homotypic fusion step of vacuole inheritance. *EMBO J.* 14:5258–5270.

Harmon, B., L.A. Chylek, Y. Liu, E.D. Mitra, A. Mahajan, E.A. Saada, B.R. Schudel, D.A. Holowka, B.A. Baird, B.S. Wilson, W.S. Hlavacek, and A.K. Singh. 2017. Timescale Separation of Positive and Negative Signaling Creates History-Dependent Responses to IgE Receptor Stimulation. *Sci. Rep.* 7:15586. doi:10.1038/s41598-017-15568-2.

Herzog, F.A., L. Braun, I. Schoen, and V. Vogel. 2016. Improved Side Chain Dynamics in MARTINI Simulations of Protein–Lipid Interfaces. *J. Chem. Theory Comput.* 12:2446–2458. doi:10.1021/acs.jctc.6b00122.

Hsu, A.-L., T.-T. Ching, G. Sen, D.-S. Wang, S. Bondada, K.S. Authi, and C.-S. Chen. 2000. Novel Function of Phosphoinositide 3-Kinase in T Cell Ca2+ Signaling. *J. Biol. Chem.* 275:16242–16250. doi:10.1074/jbc.M002077200.

Inagaki, M., T. Schmelzle, K. Yamaguchi, K. Irie, M.N. Hall, and K. Matsumoto. 1999. PDK1 Homologs Activate the Pkc1–Mitogen-Activated Protein Kinase Pathway in Yeast. *Mol. Cell. Biol.* 19:8344–8352. doi:10.1128/mcb.19.12.8344.

Jethwa, N., G.H.C. Chung, M.G. Lete, A. Alonso, R.D. Byrne, V. Calleja, and B. Larijani. 2015. Endomembrane PtdIns(3,4,5)P3 activates the PI3K-Akt pathway. *J. Cell Sci.* 128:3456–3465. doi:10.1242/jcs.172775.

Jones, E.W., G.S. Zubenko, and R.R. Parker. 1982. PEP4 gene function is required for expression of several vacuolar hydrolases in Saccharomyces cerevisiae. *Genetics*. 102:665–677. doi:10.1093/genetics/102.4.665.

Jun, Y., R.A. Fratti, and W. Wickner. 2004. Diacylglycerol and its formation by phospholipase C regulate Rab- and SNARE-dependent yeast vacuole fusion. *J. Biol. Chem.* 279:53186–53195. doi:10.1074/jbc.M411363200.

Jun, Y., N. Thorngren, V.J. Starai, R.A. Fratti, K. Collins, and W. Wickner. 2006. Reversible, cooperative reactions of yeast vacuole docking. *EMBO J.* 25:5260–5269. doi:10.1038/sj.emboj.7601413.

Jun, Y., and W. Wickner. 2007. Assays of vacuole fusion resolve the stages of docking, lipid mixing, and content mixing. *Proc. Natl. Acad. Sci. U. S. A.* 104:13010–13015. doi:10.1073/pnas.0700970104.

Jun, Y., H. Xu, N. Thorngren, and W. Wickner. 2007. Sec18p and Vam7p remodel trans-SNARE complexes to permit a lipid-anchored R-SNARE to support yeast vacuole fusion. *EMBO J.* 26:4935–4945. doi:10.1038/sj.emboj.7601915.

Karunakaran, S., T. Sasser, S. Rajalekshmi, and R.A. Fratti. 2012. SNAREs, HOPS and regulatory lipids control the dynamics of vacuolar actin during homotypic fusion in S. cerevisiae. *J. Cell Sci.* 125:1683–1692. doi:10.1242/jcs.091900.

Kassouf, N., A. Ambily, S. Watson, S. Hassock, H.S. Authi, S. Srivastava, S.P. Watson, and K.S. Authi. 2015. Phosphatidylinositol-3,4,5-trisphosphate stimulates Ca(2+) elevation and Akt phosphorylation to constitute a major mechanism of thromboxane A2 formation in human platelets. *Cell. Signal.* 27:1488–1498. doi:10.1016/j.cellsig.2015.03.008.

Kato, M., and W. Wickner. 2001. Ergosterol is required for the Sec18/ATP-dependent priming step of homotypic vacuole fusion. *EMBO J.* 20:4035–4040. doi:10.1093/emboj/20.15.4035.

Kavran, J.M., D.E. Klein, A. Lee, M. Falasca, S.J. Isakoff, E.Y. Skolnik, and M.A. Lemmon. 1998. Specificity and promiscuity in phosphoinositide binding by pleckstrin homology domains. *J. Biol. Chem.* 273:30497–30508. doi:10.1074/jbc.273.46.30497.

Khuong, T.M., R.L.P. Habets, S. Kuenen, A. Witkowska, J. Kasprowicz, J. Swerts, R. Jahn, G. van den Bogaart, and P. Verstreken. 2013. Synaptic PI(3,4,5)P3 is required for

Syntaxin1A clustering and neurotransmitter release. *Neuron*. 77:1097–1108. doi:10.1016/j.neuron.2013.01.025.

Klionsky, D.J., and S.D. Emr. 1989. Membrane protein sorting: biosynthesis, transport and processing of yeast vacuolar alkaline phosphatase. *EMBO J.* 8:2241–2250.

Krauss, M., and V. Haucke. 2007. Phosphoinositides: regulators of membrane traffic and protein function. *FEBS Lett.* 581:2105–2111. doi:10.1016/j.febslet.2007.01.089.

Laczkó-Dobos, H., A. Bhattacharjee, A.K. Maddali, A. Kincses, H. Abuammar, K. Sebők-Nagy, T. Páli, A. Dér, T. Hegedűs, G. Csordás, and G. Juhász. 2024. PtdIns4p is required for the autophagosomal recruitment of STX17 (syntaxin 17) to promote lysosomal fusion. *Autophagy*. 0. doi:10.1080/15548627.2024.2322493.

Lai, C.-L., A. Srivastava, C. Pilling, A.R. Chase, J.J. Falke, and G.A. Voth. 2013. Molecular mechanism of membrane binding of the GRP1 PH domain. *J. Mol. Biol.* 425:3073–3090. doi:10.1016/j.jmb.2013.05.026.

Lam, A.D., P. Tryoen-Toth, B. Tsai, N. Vitale, and E.L. Stuenkel. 2008. SNARE-catalyzed fusion events are regulated by Syntaxin1A-lipid interactions. *Mol. Biol. Cell*. 19:485–497. doi:10.1091/mbc.e07-02-0148.

Lawrence, G., C.C. Brown, B.A. Flood, S. Karunakaran, M. Cabrera, M. Nordmann, C. Ungermann, and R.A. Fratti. 2014. Dynamic association of the PI3P-interacting Mon1-Ccz1 GEF with vacuoles is controlled through its phosphorylation by the type 1 casein kinase Yck3. *Mol. Biol. Cell*. 25:1608–1619. doi:10.1091/mbc.E13-08-0460.

Lee, J.O., H. Yang, M.M. Georgescu, A. Di Cristofano, T. Maehama, Y. Shi, J.E. Dixon, P. Pandolfi, and N.P. Pavletich. 1999. Crystal structure of the PTEN tumor suppressor: implications for its phosphoinositide phosphatase activity and membrane association. *Cell*. 99:323–334. doi:10.1016/s0092-8674(00)81663-3.

Lemmon, M.A. 2008. Membrane recognition by phospholipid-binding domains. *Nat. Rev. Mol. Cell Biol.* 9:99–111. doi:10.1038/nrm2328.

Levina, A., K.D. Fleming, J.E. Burke, and T.A. Leonard. 2022. Activation of the essential kinase PDK1 by phosphoinositide-driven trans-autophosphorylation. *Nat. Commun.* 13:1874. doi:10.1038/s41467-022-29368-4.

Lindsay, Y., D. McCoull, L. Davidson, N.R. Leslie, A. Fairservice, A. Gray, J. Lucocq, and C.P. Downes. 2006. Localization of agonist-sensitive PtdIns(3,4,5)P3 reveals a nuclear pool that is insensitive to PTEN expression. *J. Cell Sci.* 119:5160–5168. doi:10.1242/jcs.000133.

Lingwood, D., and K. Simons. 2010. Lipid rafts as a membrane-organizing principle. *Science*. 327:46–50. doi:10.1126/science.1174621.

Maehama, T., and J.E. Dixon. 1998. The Tumor Suppressor, PTEN/MMAC1, Dephosphorylates the Lipid Second Messenger, Phosphatidylinositol 3,4,5-Trisphosphate*. *J. Biol. Chem.* 273:13375–13378. doi:10.1074/jbc.273.22.13375.

Martínez-Muñoz, G.A., and A. Peña. 2005. In situ study of K+ transport into the vacuole of Saccharomyces cerevisiae. *Yeast Chichester Engl.* 22:689–704. doi:10.1002/yea.1238.

Mayer, A., D. Scheglmann, S. Dove, A. Glatz, W. Wickner, and A. Haas. 2000. Phosphatidylinositol 4,5-bisphosphate regulates two steps of homotypic vacuole fusion. *Mol. Biol. Cell*. 11:807–817. doi:10.1091/mbc.11.3.807.

Mayer, A., and W. Wickner. 1997. Docking of yeast vacuoles is catalyzed by the Ras-like GTPase Ypt7p after symmetric priming by Sec18p (NSF). *J. Cell Biol.* 136:307–317. doi:10.1083/jcb.136.2.307.

Mayer, A., W. Wickner, and A. Haas. 1996. Sec18p (NSF)-driven release of Sec17p (alpha-SNAP) can precede docking and fusion of yeast vacuoles. *Cell*. 85:83–94. doi:10.1016/s0092-8674(00)81084-3.

Miao, B., I. Skidan, J. Yang, A. Lugovskoy, M. Reibarkh, K. Long, T. Brazell, K.A. Durugkar, J. Maki, C.V. Ramana, B. Schaffhausen, G. Wagner, V. Torchilin, J. Yuan, and A. Degterev. 2010. Small molecule inhibition of phosphatidylinositol-3,4,5-triphosphate (PIP3) binding to pleckstrin homology domains. *Proc. Natl. Acad. Sci.* 107:20126–20131. doi:10.1073/pnas.1004522107.

Miner, G.E., M.L. Starr, L.R. Hurst, R.P. Sparks, M. Padolina, and R.A. Fratti. 2016. The Central Polybasic Region of the Soluble SNARE (Soluble N-Ethylmaleimide-sensitive Factor Attachment Protein Receptor) Vam7 Affects Binding to Phosphatidylinositol 3-Phosphate by the PX (Phox Homology) Domain. *J. Biol. Chem.* 291:17651–17663. doi:10.1074/jbc.M116.725366.

Miner, G.E., K.D. Sullivan, A. Guo, B.C. Jones, L.R. Hurst, E.C. Ellis, M.L. Starr, and R.A. Fratti. 2019. Phosphatidylinositol 3,5-bisphosphate regulates the transition between trans-SNARE complex formation and vacuole membrane fusion. *Mol. Biol. Cell*. 30:201–208. doi:10.1091/mbc.E18-08-0505.

Miner, G.E., K.D. Sullivan, C. Zhang, D. Rivera-Kohr, A. Guo, L.R. Hurst, E.C. Ellis, M.L. Starr, B.C. Jones, and R.A. Fratti. 2020. Phosphatidylinositol 3,5-bisphosphate regulates Ca2+ transport during yeast vacuolar fusion through the Ca2+ ATPase Pmc1. *Traffic Cph. Den.* 21:503–517. doi:10.1111/tra.12736.

Mitra, P., Y. Zhang, L.E. Rameh, M.P. Ivshina, D. McCollum, J.J. Nunnari, G.M. Hendricks, M.L. Kerr, S.J. Field, L.C. Cantley, and A.H. Ross. 2004. A novel phosphatidylinositol(3,4,5)P3 pathway in fission yeast. *J. Cell Biol.* 166:205–211. doi:10.1083/jcb.200404150.

Naughton, F.B., A.C. Kalli, and M.S.P. Sansom. 2016. Association of Peripheral Membrane Proteins with Membranes: Free Energy of Binding of GRP1 PH Domain with Phosphatidylinositol Phosphate-Containing Model Bilayers. *J. Phys. Chem. Lett.* 7:1219–1224. doi:10.1021/acs.jpclett.6b00153.

Ni, Y., J. Sinnett-Smith, S.H. Young, and E. Rozengurt. 2013. PKD1 mediates negative feedback of PI3K/Akt activation in response to G protein-coupled receptors. *PloS One*. 8:e73149. doi:10.1371/journal.pone.0073149.

Nichols, B.J., C. Ungermann, H.R. Pelham, W.T. Wickner, and A. Haas. 1997. Homotypic vacuolar fusion mediated by t- and v-SNAREs. *Nature*. 387:199–202. doi:10.1038/387199a0.

Pesesse, X., C. Moreau, A.L. Drayer, R. Woscholski, P. Parker, and C. Erneux. 1998. The SH2 domain containing inositol 5-phosphatase SHIP2 displays phosphatidylinositol 3,4,5-trisphosphate and inositol 1,3,4,5-tetrakisphosphate 5-phosphatase activity. *FEBS Lett.* 437:301–303. doi:10.1016/s0014-5793(98)01255-1.

Posor, Y., W. Jang, and V. Haucke. 2022. Phosphoinositides as membrane organizers. *Nat. Rev. Mol. Cell Biol.* 23:797–816. doi:10.1038/s41580-022-00490-x.

Price, A., D. Seals, W. Wickner, and C. Ungermann. 2000a. The docking stage of yeast vacuole fusion requires the transfer of proteins from a cis-SNARE complex to a Rab/Ypt protein. *J. Cell Biol.* 148:1231–1238. doi:10.1083/jcb.148.6.1231.

Price, A., W. Wickner, and C. Ungermann. 2000b. Proteins needed for vesicle budding from the Golgi complex are also required for the docking step of homotypic vacuole fusion. *J. Cell Biol.* 148:1223–1229. doi:10.1083/jcb.148.6.1223.

Pringle, J.R., A.E. Adams, D.G. Drubin, and B.K. Haarer. 1991. Immunofluorescence methods for yeast. *Methods Enzymol.* 194:565–602. doi:10.1016/0076-6879(91)94043-c.

Qiu, Q.-S., and R.A. Fratti. 2010. The Na+/H+ exchanger Nhx1p regulates the initiation of Saccharomyces cerevisiae vacuole fusion. *J. Cell Sci.* 123:3266–3275. doi:10.1242/jcs.067637.

Reese, C., F. Heise, and A. Mayer. 2005. Trans-SNARE pairing can precede a hemifusion intermediate in intracellular membrane fusion. *Nature*. 436:410–414. doi:10.1038/nature03722.

Reese, C., and A. Mayer. 2005. Transition from hemifusion to pore opening is rate limiting for vacuole membrane fusion. *J. Cell Biol.* 171:981–990. doi:10.1083/jcb.200510018.

Riehle, R.D., S. Cornea, and A. Degterev. 2013. Role of phosphatidylinositol 3,4,5-trisphosphate in cell signaling. *Adv. Exp. Med. Biol.* 991:105–139. doi:10.1007/978-94-007-6331-9_7.

Ronan, B., O. Flamand, L. Vescovi, C. Dureuil, L. Durand, F. Fassy, M.-F. Bachelot, A. Lamberton, M. Mathieu, T. Bertrand, J.-P. Marquette, Y. El-Ahmad, B. Filoche-Romme, L. Schio, C. Garcia-Echeverria, H. Goulaouic, and B. Pasquier. 2014. A highly potent and selective Vps34 inhibitor alters vesicle trafficking and autophagy. *Nat. Chem. Biol.* 10:1013–1019. doi:10.1038/nchembio.1681.

Sahan, A.Z., M. Chen, Q. Su, Q. Li, D. Wang, and J. Zhang. 2025. Lysosomal PIP3 revealed by genetically encoded lipid biosensors. *Proc. Natl. Acad. Sci.* 122:e2426929122. doi:10.1073/pnas.2426929122.

Sasser, T., Q.-S. Qiu, S. Karunakaran, M. Padolina, A. Reyes, B. Flood, S. Smith, C. Gonzales, and R.A. Fratti. 2012. Yeast lipin 1 orthologue pah1p regulates vacuole homeostasis and membrane fusion. *J. Biol. Chem.* 287:2221–2236. doi:10.1074/jbc.M111.317420.

Sasser, T.L., G. Lawrence, S. Karunakaran, C. Brown, and R.A. Fratti. 2013. The yeast ATP-binding cassette (ABC) transporter Ycf1p enhances the recruitment of the soluble SNARE Vam7p to vacuoles for efficient membrane fusion. *J. Biol. Chem.* 288:18300–18310. doi:10.1074/jbc.M112.441089.

Scott, J.H., and R. Schekman. 1980. Lyticase: endoglucanase and protease activities that act together in yeast cell lysis. *J. Bacteriol.* 142:414–423. doi:10.1128/jb.142.2.414-423.1980.

Seals, D.F., G. Eitzen, N. Margolis, W.T. Wickner, and A. Price. 2000. A Ypt/Rab effector complex containing the Sec1 homolog Vps33p is required for homotypic vacuole fusion. *Proc. Natl. Acad. Sci. U. S. A.* 97:9402–9407. doi:10.1073/pnas.97.17.9402.

Slusarewicz, P., Z. Xu, K. Seefeld, A. Haas, and W.T. Wickner. 1997. I2B is a small cytosolic protein that participates in vacuole fusion. *Proc. Natl. Acad. Sci. U. S. A.* 94:5582–5587. doi:10.1073/pnas.94.11.5582.

Sparks, R.P., A.S. Arango, J.L. Jenkins, W.C. Guida, E. Tajkhorshid, C.E. Sparks, J.D. Sparks, and R.A. Fratti. 2020. An Allosteric Binding Site on Sortilin Regulates the Trafficking of VLDL, PCSK9, and LDLR in Hepatocytes. *Biochemistry*. 59:4321–4335. doi:10.1021/acs.biochem.0c00741.

Sparks, R.P., A.S. Arango, M.L. Starr, Z.L. Aboff, L.R. Hurst, D.A. Rivera-Kohr, C. Zhang, K.A. Harnden, J.L. Jenkins, W.C. Guida, E. Tajkhorshid, and R.A. Fratti. 2019. A small-molecule competitive inhibitor of phosphatidic acid binding by the AAA+ protein NSF/Sec18 blocks the SNARE-priming stage of vacuole fusion. *J. Biol. Chem.* 294:17168–17185. doi:10.1074/jbc.RA119.008865.

Sparks, R.P., J.L. Jenkins, G.E. Miner, Y. Wang, W.C. Guida, C.E. Sparks, R.A. Fratti, and J.D. Sparks. 2016. Phosphatidylinositol (3,4,5)-trisphosphate binds to sortilin and competes with neurotensin: Implications for very low density lipoprotein binding. *Biochem. Biophys. Res. Commun.* 479:551–556. doi:10.1016/j.bbrc.2016.09.108.

Sparks, R.P., W. Lawless, A.S. Arango, E. Tajkhorshid, and R.A. Fratti. 2022. Use of Microscale Thermophoresis to Measure Protein-Lipid Interactions. *J. Vis. Exp. JoVE*. doi:10.3791/60607.

Starai, V.J., Y. Jun, and W. Wickner. 2007. Excess vacuolar SNAREs drive lysis and Rab bypass fusion. *Proc. Natl. Acad. Sci. U. S. A.* 104:13551–13558. doi:10.1073/pnas.0704741104.

Starr, M.L., and R.A. Fratti. 2019. The Participation of Regulatory Lipids in Vacuole Homotypic Fusion. *Trends Biochem. Sci.* 44:546–554. doi:10.1016/j.tibs.2018.12.003.

Starr, M.L., L.R. Hurst, and R.A. Fratti. 2016. Phosphatidic Acid Sequesters Sec18p from cis-SNARE Complexes to Inhibit Priming. *Traffic Cph. Den.* 17:1091–1109. doi:10.1111/tra.12423.

Starr, M.L., R.P. Sparks, A.S. Arango, L.R. Hurst, Z. Zhao, M. Lihan, J.L. Jenkins, E. Tajkhorshid, and R.A. Fratti. 2019. Phosphatidic acid induces conformational changes in

Sec18 protomers that prevent SNARE priming. *J. Biol. Chem.* 294:3100–3116. doi:10.1074/jbc.RA118.006552.

Stefan, C.J., A. Audhya, and S.D. Emr. 2002. The yeast synaptojanin-like proteins control the cellular distribution of phosphatidylinositol (4,5)-bisphosphate. *Mol. Biol. Cell*. 13:542–557. doi:10.1091/mbc.01-10-0476.

Stroupe, C., K.M. Collins, R.A. Fratti, and W. Wickner. 2006. Purification of active HOPS complex reveals its affinities for phosphoinositides and the SNARE Vam7p. *EMBO J.* 25:1579–1589. doi:10.1038/sj.emboj.7601051.

Thorngren, N., K.M. Collins, R.A. Fratti, W. Wickner, and A.J. Merz. 2004. A soluble SNARE drives rapid docking, bypassing ATP and Sec17/18p for vacuole fusion. *EMBO J.* 23:2765–2776. doi:10.1038/sj.emboj.7600286.

Traynor-Kaplan, A.E., A.L. Harris, B.L. Thompson, P. Taylor, and L.A. Sklar. 1988. An inositol tetrakisphosphate-containing phospholipid in activated neutrophils. *Nature*. 334:353–356. doi:10.1038/334353a0.

Tu-Sekine, B., H. Goldschmidt, and D.M. Raben. 2015. Diacylglycerol, phosphatidic acid, and their metabolic enzymes in synaptic vesicle recycling. *Adv. Biol. Regul.* 57:147–152. doi:10.1016/j.jbior.2014.09.010.

Uetz, P., L. Giot, G. Cagney, T.A. Mansfield, R.S. Judson, J.R. Knight, D. Lockshon, V. Narayan, M. Srinivasan, P. Pochart, A. Qureshi-Emili, Y. Li, B. Godwin, D. Conover, T. Kalbfleisch, G. Vijayadamodar, M. Yang, M. Johnston, S. Fields, and J.M. Rothberg. 2000. A comprehensive analysis of protein-protein interactions in Saccharomyces cerevisiae. *Nature*. 403:623–627. doi:10.1038/35001009.

Ungermann, C., K. Sato, and W. Wickner. 1998. Defining the functions of trans-SNARE pairs. *Nature*. 396:543–548. doi:10.1038/25069.

Wang, L., A.J. Merz, K.M. Collins, and W. Wickner. 2003. Hierarchy of protein assembly at the vertex ring domain for yeast vacuole docking and fusion. *J. Cell Biol.* 160:365–374. doi:10.1083/jcb.200209095.

Wang, L., E.S. Seeley, W. Wickner, and A.J. Merz. 2002. Vacuole fusion at a ring of vertex docking sites leaves membrane fragments within the organelle. *Cell*. 108:357–369. doi:10.1016/s0092-8674(02)00632-3.

Whitman, M., C.P. Downes, M. Keeler, T. Keller, and L. Cantley. 1988. Type I phosphatidylinositol kinase makes a novel inositol phospholipid, phosphatidylinositol-3-phosphate. *Nature*. 332:644–646. doi:10.1038/332644a0.

Whitman, M., D.R. Kaplan, B. Schaffhausen, L. Cantley, and T.M. Roberts. 1985. Association of phosphatidylinositol kinase activity with polyoma middle-T competent for transformation. *Nature*. 315:239–242. doi:10.1038/315239a0.

Xie, S., N. Naslavsky, and S. Caplan. 2015. Diacylglycerol kinases in membrane trafficking. *Cell. Logist.* 5:e1078431. doi:10.1080/21592799.2015.1078431.

Yamamoto, E., J. Domański, F.B. Naughton, R.B. Best, A.C. Kalli, P.J. Stansfeld, and M.S.P. Sansom. 2020. Multiple lipid binding sites determine the affinity of PH domains for phosphoinositide-containing membranes. *Sci. Adv.* 6:eaay5736. doi:10.1126/sciadv.aay5736.

Yu, J.W., and M.A. Lemmon. 2001. All phox homology (PX) domains from Saccharomyces cerevisiae specifically recognize phosphatidylinositol 3-phosphate. *J. Biol. Chem.* 276:44179–44184. doi:10.1074/jbc.M108811200.

Zhang, C., J.D. Calderin, L.R. Hurst, Z.D. Gokbayrak, M.R. Hrabak, A. Balutowski, D.A. Rivera-Kohr, T.D.D. Kazmirchuk, C.L. Brett, and R.A. Fratti. 2024. Sphingolipids containing very long-chain fatty acids regulate Ypt7 function during the tethering stage of vacuole fusion. *J. Biol. Chem.* 107808. doi:10.1016/j.jbc.2024.107808.

Zhang, C., Y. Feng, A. Balutowski, G.E. Miner, D.A. Rivera-Kohr, M.R. Hrabak, K.D. Sullivan, A. Guo, J.D. Calderin, and R.A. Fratti. 2022. The interdependent transport of yeast vacuole Ca2+ and H+ and the role of Phosphatidylinositol 3,5-bisphosphate. *J. Biol. Chem.* 102672. doi:10.1016/j.jbc.2022.102672.

Zhu, H., M. Bilgin, R. Bangham, D. Hall, A. Casamayor, P. Bertone, N. Lan, R. Jansen, S. Bidlingmaier, T. Houfek, T. Mitchell, P. Miller, R.A. Dean, M. Gerstein, and M. Snyder. 2001. Global Analysis of Protein Activities Using Proteome Chips. *Science*. 293:2101–2105. doi:10.1126/science.1062191.

Figures and Legends

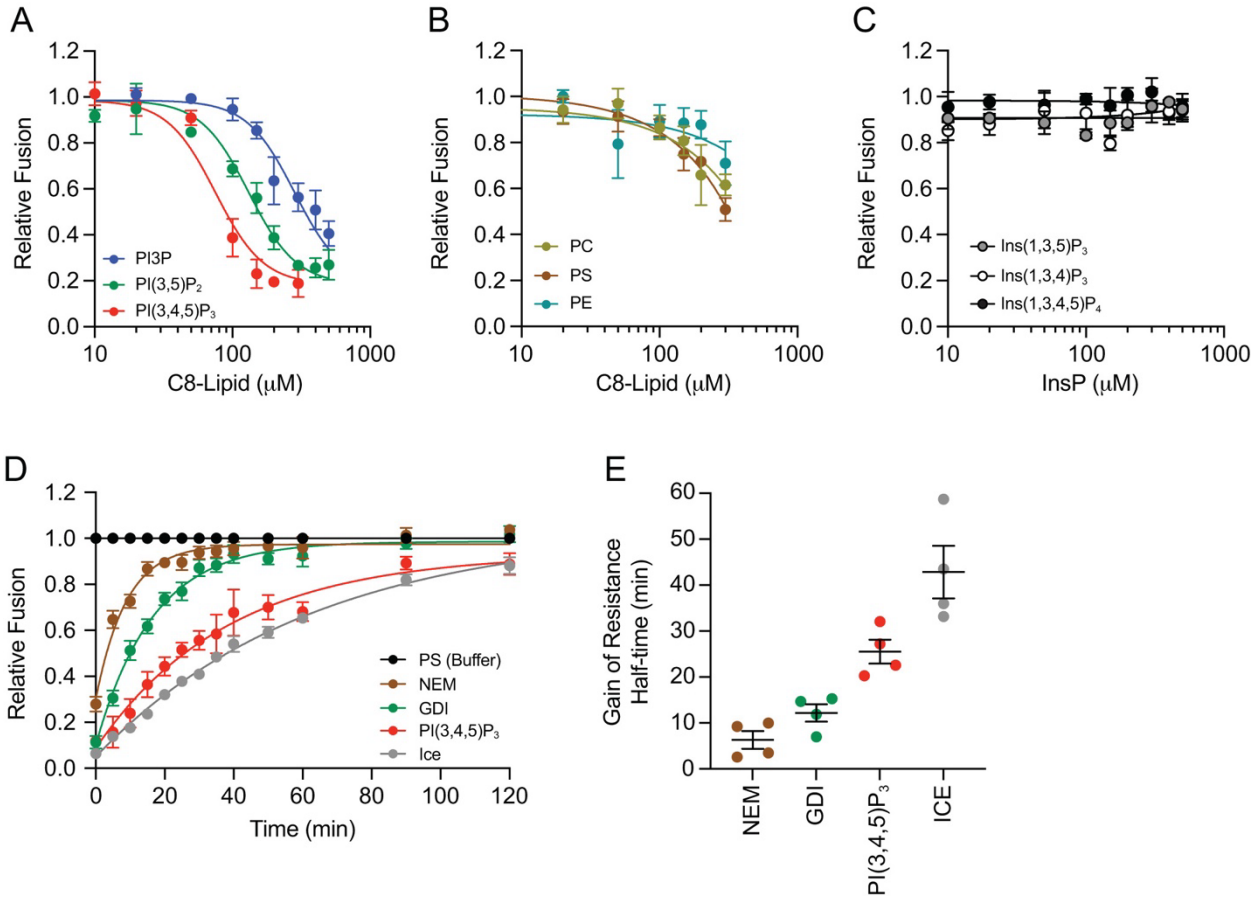

Figure 1. C8-PI(3,4,5)P_3 inhibits fusion after vacuole tethering.

Fusion reactions were treated with buffer alone or curves of: C8-PI3P, C8-PI(3,5)P_2 and C8-PI(3,4,5)P_3 **(A);** C8-PC, C8-PS and C8-PE **(B);** Ins(1,3,5)P_3, Ins(1,3,4)P_3 and Ins(1,3,4,5)P_4 **(C)** and incubated for 90 min at 27ºC. Fusion was normalized to the maximum fusion (buffer alone) set to 1 for each curve. Data show the mean and SE (n≥3) and fit to one-phase decay curves. IC_{50} values were determined using Graphpad Prism-10. **(D)** Gain of resistance fusion reactions were performed with PS buffer, 1 mM NEM, 2 μM GDI or 150 μM C8-PI(3,4,5)P_3. Individual reactions were treated with reagents/buffer at the indicated time points. A second set of buffer-treated reactions were placed on ice at the indicated times. Reactions were incubated for a total of 120 min at 27ºC. Fusion levels for each reaction was normalized to the untreated control at each time point set to 1. Data show the average and SE (n≥3) and fit to one-phase decay curves. **(E)** Calculated half-times of resistance from assays in **(D)**. Error bars represent SEM (n=3).

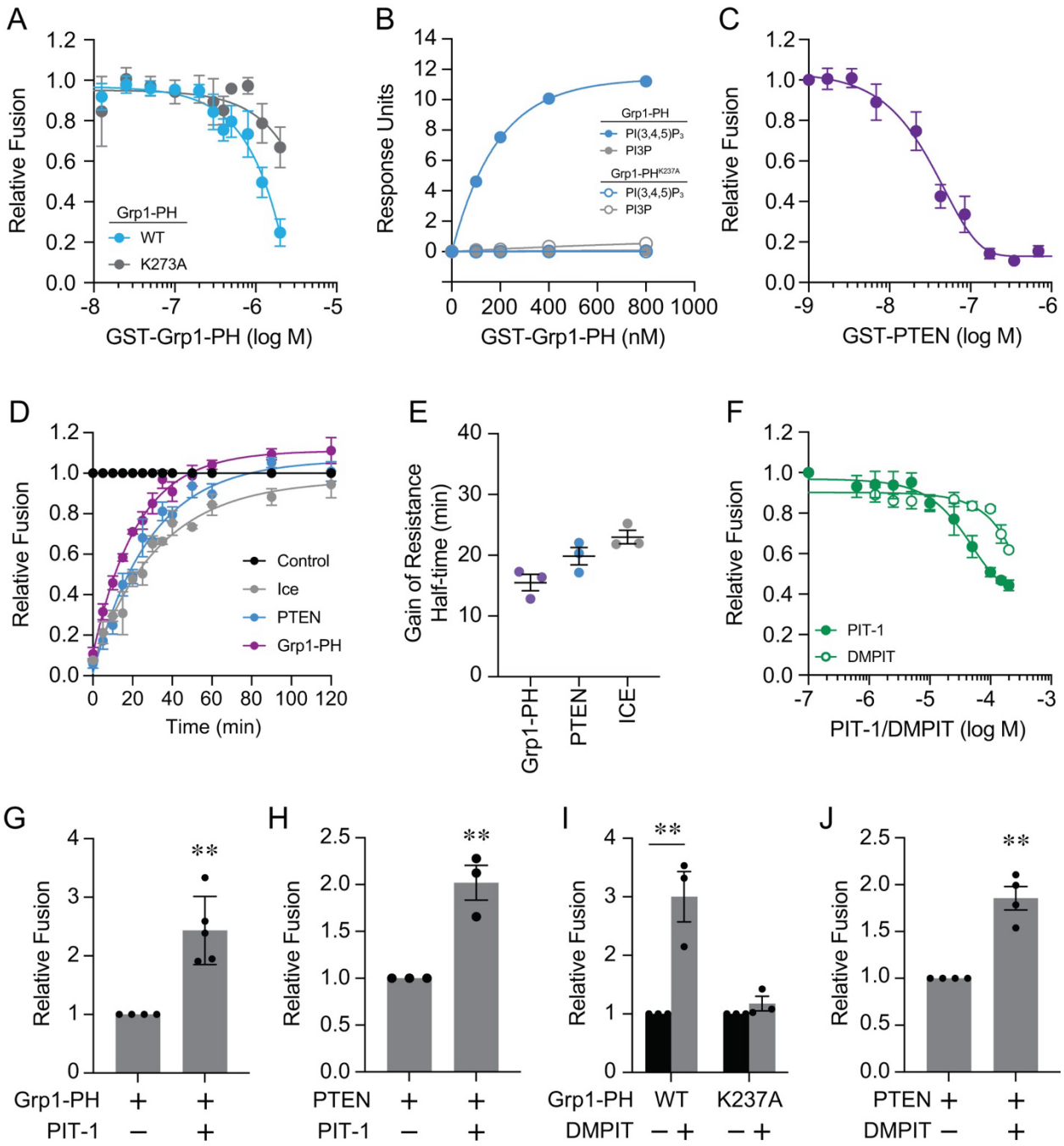

Figure 2. PIP3 specific reagents inhibit vacuole fusion.

(A) Fusion reactions were treated with buffer or curves of GST-Grp1-PH or GST-Grp1-PH^{K237A} and incubated for 90 min at 27ºC. Each curve was normalized to the maximum fusion (no treatment) set to 1. Data shows the averages and SE (n≥3). Data sets were fit to one-phase decay curves and IC_{50} values were determined using Graphpad Prism-10. **(B)** BLI of GST-Grp1-PH and GST-Grp1-PH^{K237A} binding to b-PI(3,4,5)P_3 or b-PI3P. **(C)** Dose curve of GST-PTEN inhibition of

fusion as described in (A). **(D)** Gain of resistance fusion reactions were performed with buffer, 1 mM NEM, 2 μM GDI, 2 μM GST-Grp1-PH, or 200 nM PTEN. Reagents/buffer were added at the indicated times. A second set of untreated reactions was placed on ice at each timepoint. Fusion reactions were incubated for a total of 120 min and fusion for each reaction was normalized to the untreated control for the each timepoint at 27°C set to 1. Data sets show the average and SE and fit to one-phase decay curves ($n \geq 3$). **(E)** Calculated half-times of resistance from assays in **(D)**. **(F)** Dose curves of PIT-1 and 3,5-dimethyl PIT-1 (DMPIT) on vacuole fusion. Fusion inhibition by 2.3 μM Grp1-PH **(G)** or 200 nM PTEN **(H)** was rescued with 200 μM PIT-1. Fusion efficiency was normalized to Grp1-PH or PTEN set to 1. **(I)** Fusion inhibition by Grp1-PH and Grp1-PH^{K237A} (2.3 μM) in the presence or absence of 200 μM DMPIT. Fusion efficiency was normalized to Grp1-PH or Grp1-PH^{K237A} alone set to 1. **(J)** Fusion inhibition by 200 nM PTEN was rescued with 200 μM DMPIT. Fusion efficiency was normalized to PTEN alone set to 1. Error bars represent mean ± SE (n=3). In panels D-G, significance was determined unpaired two-tailed t-test. $^{**}p<0.01$.

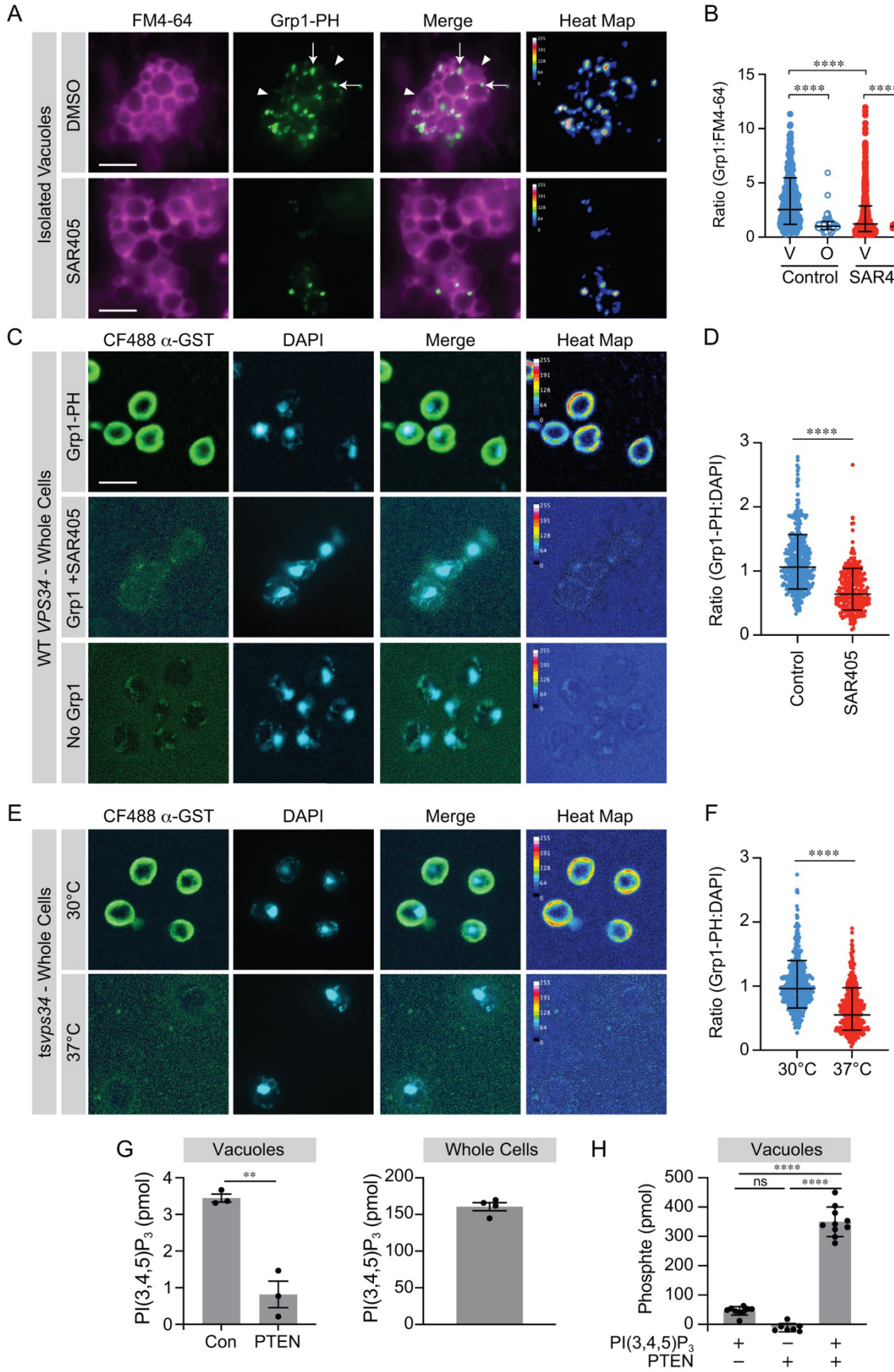
A
FM4-64
Grp1-PH
Merge
Heat Map
Isolated Vacuoles
DMSO
SAR405
B
Ratio (Grp1:FM4-64)
****
V
O
Control
SAR405
C
CF488 α-GST
DAPI
WT VPS34 - Whole Cells
Grp1-PH
Grp1 +SAR405
No Grp1
D
Ratio (Grp1-PH:DAPI)
Control
SAR405
E
tsvps34 - Whole Cells
30°C
37°C
F
G
Vacuoles
Whole Cells
PI(3,4,5)P3 (pmol)
**
Con
PTEN
H
Phosphte (pmol)
ns
PI(3,4,5)P3
PTEN

Figure 3. PI(3,4,5)P_3 is made by Vps34 and localizes at the vertices microdomains. Docking reactions were incubated for 30 min at 27ºC with 150 nM GST-Grp1-PH to mark PI(3,4,5)P_3. Grp1-PH was visualized by adding CF488-anti GST polyclonal antibody at the end of the reaction and 5 µM FM4-64 to label entire vacuoles. Vacuoles were pelleted to remove excess antibody and resuspended in PS buffer. **(A)** Docking reactions were treated with 200 µM SAR405 or DMSO and prepared for fluorescence microscopy. **(B)** Quantitation of ratiometric fluorescence intensities of vertices (V) and outer edge (O) in panel A. Data points were pooled from multiple experiments and each experiment contained ratios from 10 or more fields with 10-15 clusters made of ≥5 vacuoles (n>500 vertices and >200 outer edges per condition). Error bars represent geometric means ± geometric SD (n=3). Significance was determined using one-way ANOVA for multiple comparisons and Tukey's test for individual *p*-values. ****$p<0.0001$. **(C)** Mid-log cells were fixed and spheroplasted to detect PI(3,4,5)P_3. Spheroplasts were incubated with 10 µM GST-Grp1-PH or buffer followed by CF488 anti-GST antibody. Samples were mounted on slides with Fluoromount-G with DAPI to label nuclei. Separate samples were incubated with ant-GST in the absence of Grp1-PH. **(D)** Quantitation of plasma membrane labeling with CF488-Grp1-PH. Ratios of maximum fluorescence intensities (CF488:DAPI) were determined for ≥100 cells per condition per experiment (n=4). Significance was determined using unpaired two-tailed t-test. ****$p<0.0001$. **(E)** ts*vps34* expressing cells were grown at 30°C or 37°C and processed as described above. **(F)** Quantitation of CF488-Grp1-PH labeling was determined for both temperatures as described (n=3). Significance was determined using unpaired two-tailed t-test. ****$p<0.0001$. **(G)** Quantitation of vacuole PI(3,4,5)P_3 was performed using an ELISA kit. Fusion reactions were treated with 150 nM PTEN or buffer and incubated for 30 min at 27°C. Membranes were pelleted, and lipids were extracted as described. Bars represent mean ± SE (n=3). Significance was determined by unpaired two-tailed t-test. **$p<0.01$. **(H)** Phosphatase activity assay of PTEN (300 nM) and C8-PI(3,4,5)P_3 (3 nM) for 30 min at RT. The assays were performed using a malachite green assay kit. Bars represent mean ± SE (n=3). Significance was determined using one-way ANOVA and Tukey's for individual *p*-values. ****$p<0.0001$. Scale bars: 5 µm.

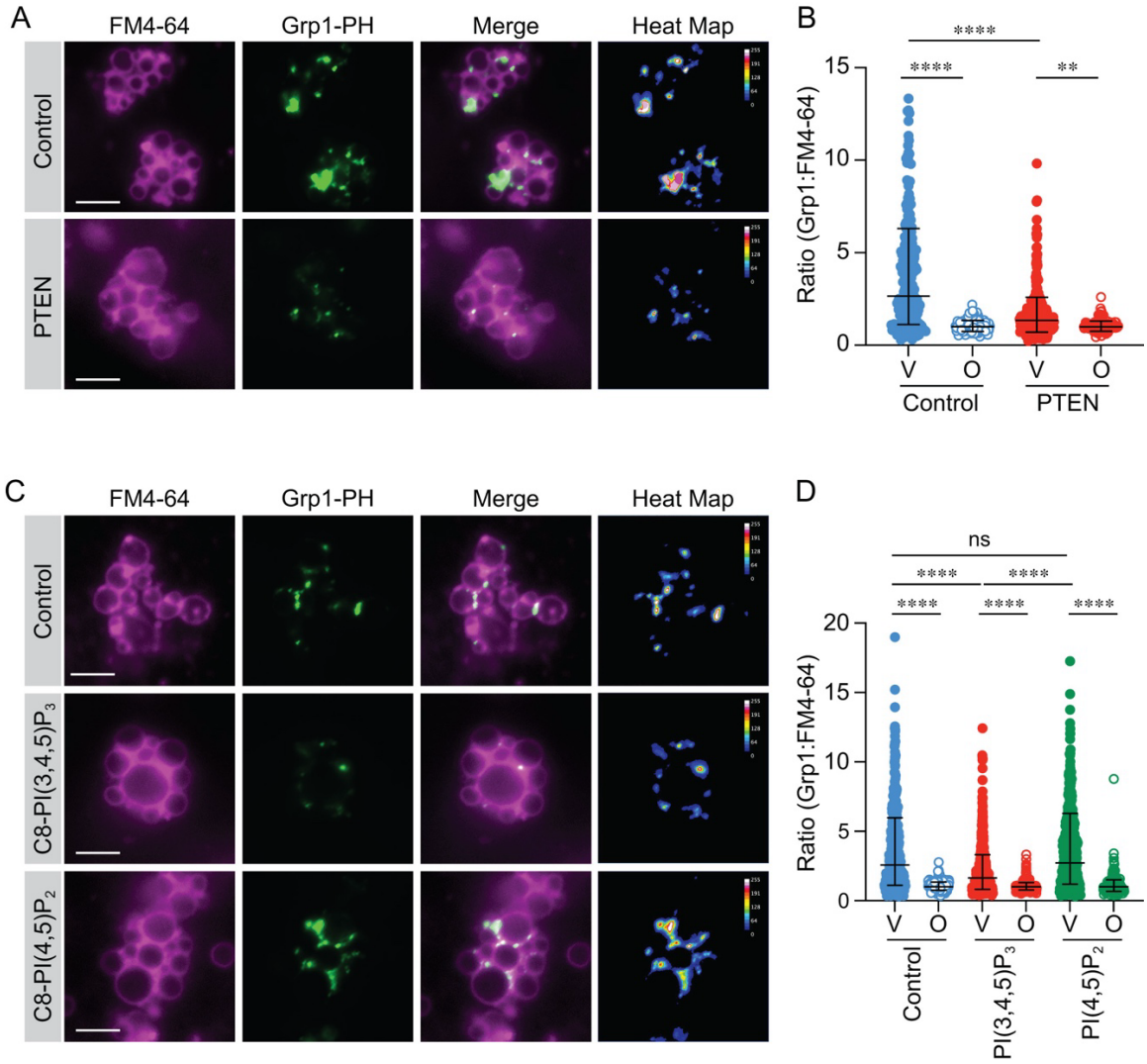

Figure 4. PI(3,4,5)P_3 competes for Grp1-PH binding

(A) Docking reactions were treated with 50 nM PTEN or PS buffer (Control). At the end of the incubation period, reactions were placed on ice, labeled with FM4-64 and prepared for fluorescence microscopy as described. **(B)** Quantitation of ratiometric fluorescence intensities of vertices (V) and outer edge (O) in panel A. Data points were pooled from multiple experiments as described in Figure 3. **(C)** Docking reactions were performed with 300 nM C8-PI(4,5)$_2$, 300 nM C8-PI(3,4,5)P_3, or buffer to compete for GST-Grp1-PH labeling. **(D)** Quantitation of ratiometric fluorescence intensities of vertices (V) and outer edge (O) in panel C. Data points were pooled from multiple experiments as described in Figure 3. Error bars represent geometric means ± geometric SD (n=3). Significance was determined using one-way ANOVA for multiple comparisons and Tukey's test for individual *p*-values. ****$p<0.0001$. ns, not significant. Scale bars: 5 µm.

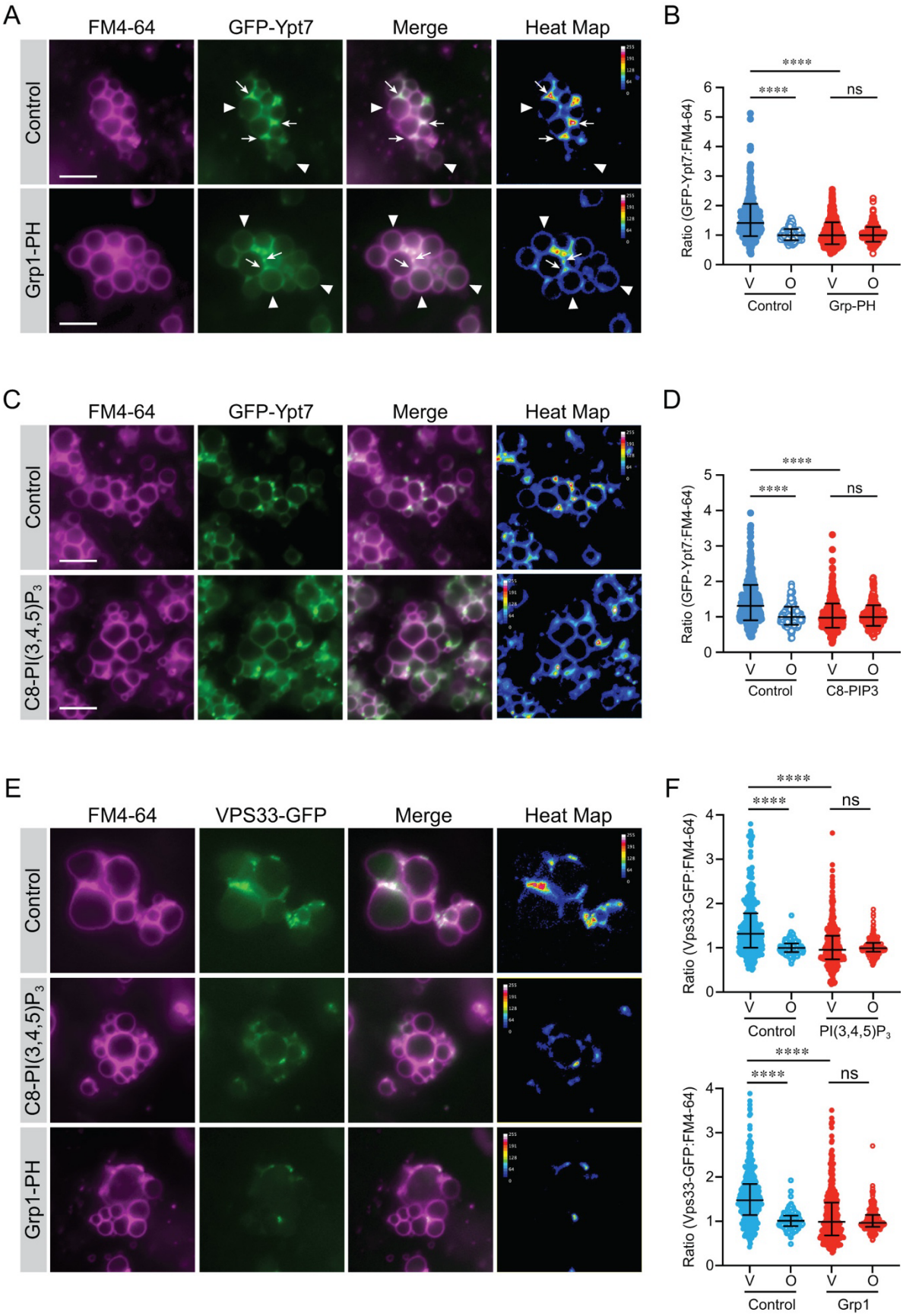
A
FM4-64
GFP-Ypt7
Merge
Heat Map
Control
Grp1-PH
B
Ratio (GFP-Ypt7:FM4-64)
****
****
ns
V
O
V
O
Control
Grp-PH
C
FM4-64
GFP-Ypt7
Merge
Heat Map
Control
C8-PI(3,4,5)P3
D
Ratio (GFP-Ypt7:FM4-64)
****
****
ns
V
O
V
O
Control
C8-PIP3
E
FM4-64
VPS33-GFP
Merge
Heat Map
Control
C8-PI(3,4,5)P3
Grp1-PH
F
Ratio (Vps33-GFP:FM4-64)
****
****
ns
V
O
V
O
Control
PI(3,4,5)P3
Ratio (Vps33-GFP:FM4-64)
****
****
ns
V
O
V
O
Control
Grp1

Figure 5. Grp1-PH blocks vertex enrichment of GFP-Ypt7 and Vps33-GFP

(A) Docking reactions with vacuoles containing GFP-Ypt7 were treated with unlabeled 2 μM Grp1-PH to inhibit fusion or buffer and incubated for 30 min at 27°C. At the end of the incubation period, reactions were prepared for fluorescence microscopy. **(B)** Quantitation of ratiometric fluorescence intensities of vertices (V) and outer edge (O) in panel A. **(C)** Docking reactions with GFP-Ypt7 vacuoles were treated with 250 μM C8-PI(3,4,5)P_3 to inhibit fusion or buffer and incubated for 30 min at 27ºC. **(D)** Quantitation of ratiometric fluorescence intensities of vertices (V) and outer edge (O) in panel C. Data points were pooled from multiple experiments as described. Error bars represent geometric means ± geometric SD (n=3). Significance was determined using one-way ANOVA for multiple comparisons and Tukey's post-hoc test was used for individual *p*-values. ****$p<0.0001$. **(E)** Docking reactions were performed with vacuoles with Vps33-GFP in the presence buffer (control), 250 μM C8-PI(3,4,5)P_3 or 2 μM Grp1-PH At the end of the incubation period, reactions were processed for fluorescence microscopy as described above. **(F)** Quantitation of ratiometric fluorescence intensities of vertices (V) and outer edge (O) in panel (E). Error bars represent geometric means ± geometric SD (n=3). Significance was determined using one-way ANOVA for multiple comparisons and Tukey's post-hoc test for individual *p*-values. ****$p<0.0001$; Scale bars: 5 μm.

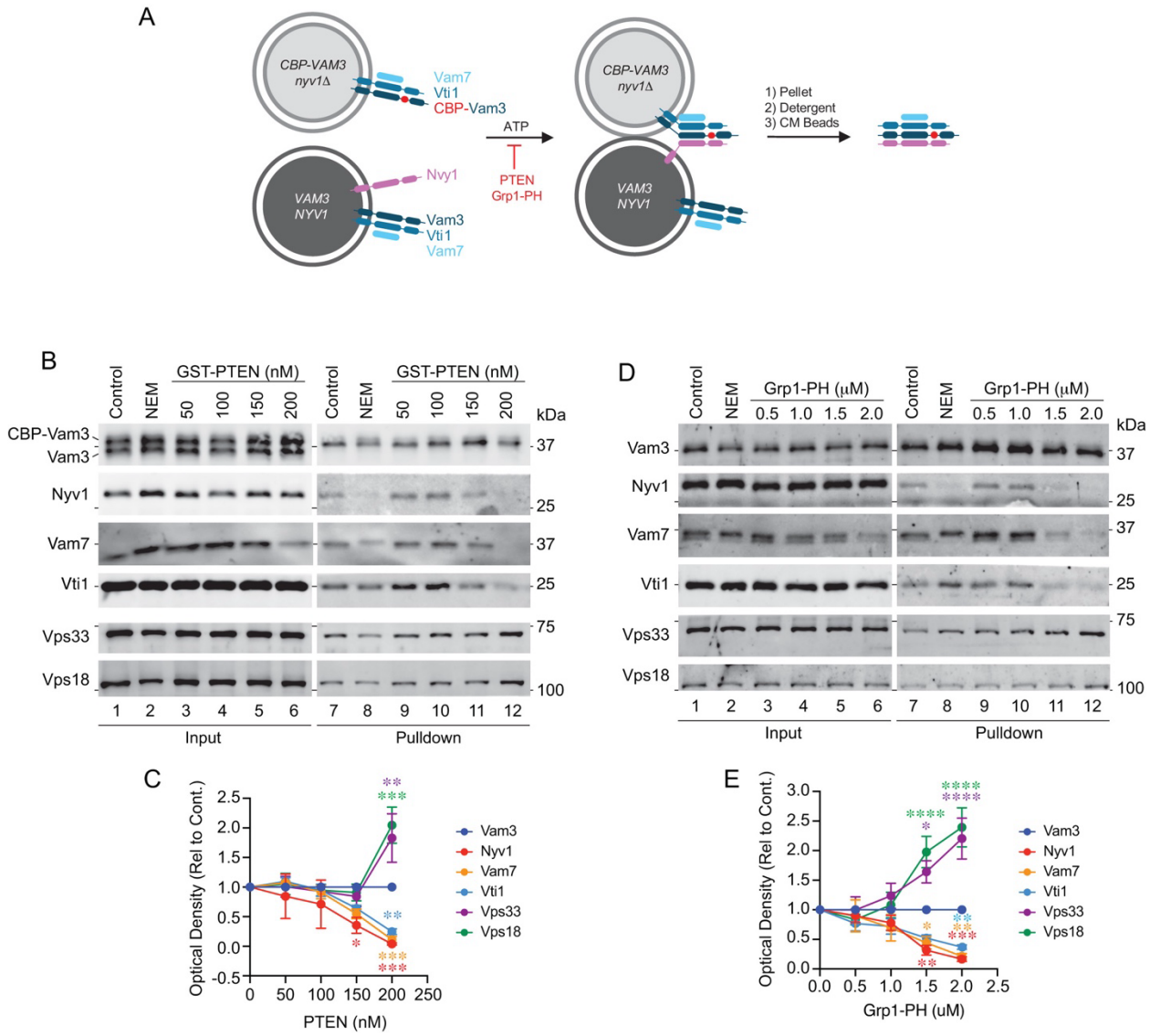

Figure 6. PI(3,4,5)P3 affects trans-SNARE pairing.

(A) Trans-SNARE isolation schematic. **(B)** Fusion reactions were treated with buffer (Control), 2 mM NEM, or GST-PTEN at the indicated concentrations. Reactions were incubated for 60 min at 27°C. Protein complexes containing CBP-Vam3 were isolated with calmodulin beads. Proteins were resolved by SDS-PAGE and processed for immunoblotting for Vam3, Nyv1, Vam7, Vti1, Vps33 and Vps18. **(C)** Quantitation of proteins bound to CBP-Vam3 in the presence of PTEN. Data represents mean and SEM (n=3). Significance was determined using one-way ANOVA for multiple comparisons and Šidák's test for pairwise comparisons between CBP-Vam3 and specified proteins for individual *p*-values. **(D)** Reactions were treated with buffer (Control), 2 mM

NEM, or GST-Grp1-PH at the indicated concentrations and processed as described above. **(E)** Quantitation of CBP-Vam3 interactions as described above. Data represents mean and SEM (n=3). *p<0.05, **p<0.01, ***p<0.001, ****p<0.0001.

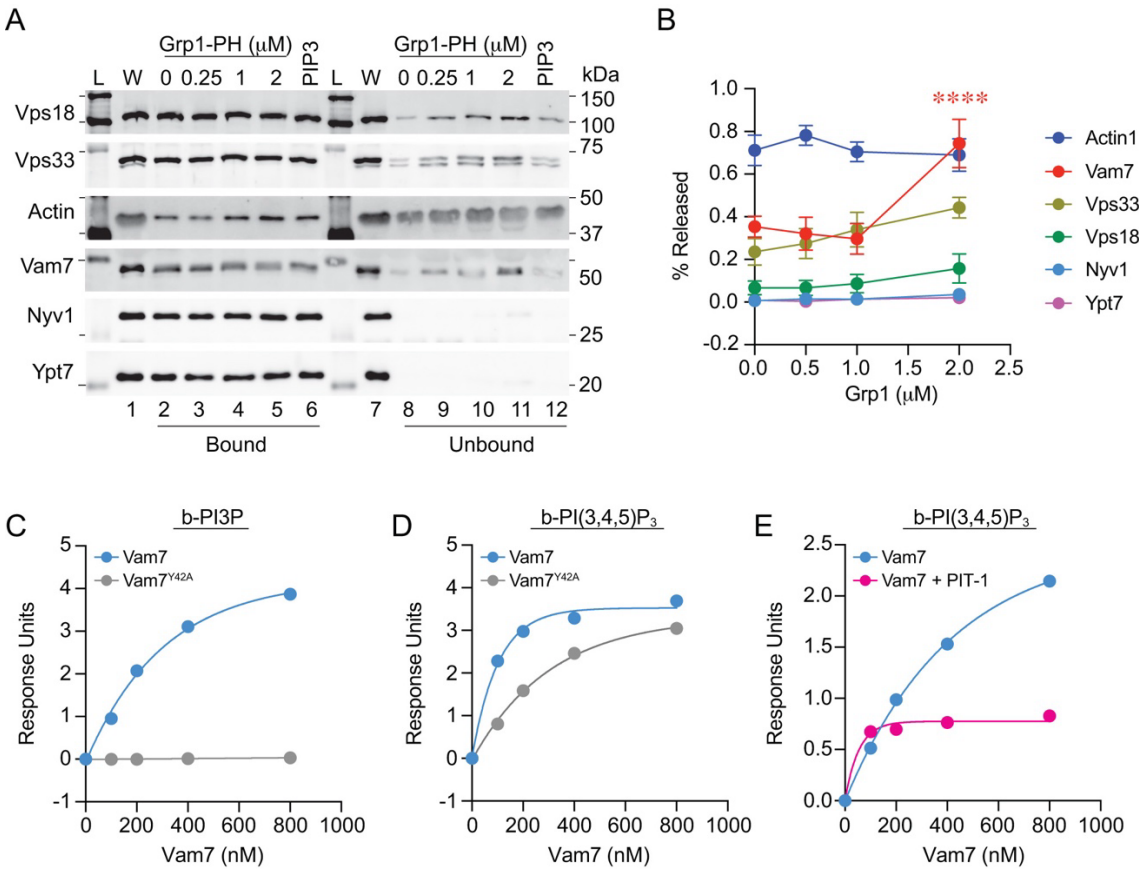

Vam7 Interact with PI(3,4,5)P_3

(A) Fusion reactions were treated with buffer (Control) or GST-Grp1-PH at the indicated concentrations. Reactions were incubated for 60 min at 27°C. Membrane-bound and unbound proteins were separated by centrifugation (16,000, 10 min, 4°C) into unbound and bound fractions. Pellets were resuspended in PS buffer to match the starting volumes. Bound and unbound fractions were mixed with SDS-loading buffer and processed for immunoblotting for Actin, Nyv1, Vam7, Ypt7, Vps33 and Vps18. **(B)** Quantitation of proteins released from vacuoles in the presence of Grp1-PH. Data represents mean and SE (n=4). Significance was determined using one-way ANOVA for multiple comparisons and Šidák's test for pairwise comparisons for individual *p*-values. ****$p<0.0001$. L, ladder; W, whole reaction. **(C-D)** BLI binding curves of b-PI3P (C) or b-PI(3,4,5)P3 (D) in response units versus protein concentrations of Vam7 and $Vam7^{Y42A}$. **(E)** BLI binding curves of PIT-1 (200 μM) inhibition of b-PI(3,4,5)P_3 binding Vam7.